INTERNATIONAL JOURNAL FOR NUMERICAL METHODS IN ENGINEERING
Int. J. Numer. Meth. Engng 2010; **00**:1–27
Published online in Wiley InterScience (www.interscience.wiley.com). DOI: 10.1002/nme

A new multi-scale dispersive gradient elasticity model with micro-inertia: Formulation and $\mathscr{C}^0$-finite element implementation

Dario De Domenico [1*], Harm Askes [2]

[1] *Department PAU, University Mediterranea of Reggio Calabria, via Melissari, Reggio Calabria 89124, Italy*
[2] *Department of Civil and Structural Engineering, University of Sheffield, Mappin Street, Sheffield S1 3JD, UK*

SUMMARY

Motivated by nano-scale experimental evidence on the dispersion characteristics of materials with a lattice structure, a new multi-scale gradient elasticity model is developed. In the framework of gradient elasticity, the *simultaneous* presence of acceleration- and strain-gradients has been denoted as *dynamic consistency*. This model represents an extension of an earlier dynamically consistent model with an additional micro-inertia contribution to improve the dispersion behaviour. The model can therefore be seen as an enhanced dynamic extension of the Aifantis 1992 strain-gradient theory for statics obtained by including two acceleration gradients in addition to the strain gradient. Compared to the previous dynamically consistent model, the additional micro-inertia term is found to improve the prediction of wave dispersion significantly and, more importantly, requires *no extra computational cost*. The fourth-order equations are rewritten in two sets of symmetric second-order equations so that $\mathscr{C}^0$-continuity is sufficient in the finite element implementation. Two sets of unknowns are identified as the *microstructural* and *macrostructural* displacements, thus highlighting the multi-scale nature of the present formulation. The associated energy functionals and variationally consistent boundary conditions are presented, after which the finite element equations are derived. Considerable improvements over previous gradient models are observed as confirmed by two numerical examples.

Received . . .

KEY WORDS: Wave dispersion; Gradient elasticity; Multiscale; Finite element methods; Dynamical systems; Generalised continuum

1. INTRODUCTION

Classical continuum field theories do not suffice to reliably capture certain mechanical phenomena. Experimental evidence and physical observations point out some intrinsic drawbacks and limitations of the classical theory of elasticity in a number of problems, e.g. to define stress and strain fields around sharp crack-tips or dislocation cores, the description of size effects and dispersive wave propagation. The common characteristic of the above problems in which classical continuum mechanics fails resides in the fact that nonlocal interactions play a major role in the deformation process. The applicability of the standard continuum mechanics of Cauchy is indeed closely related to the relevant length- and time-scales because it is implicitly assumed that the external length-scales and time-scales are much larger than those of the dominant heterogeneities. If the external length scale is of the same order of magnitude as the internal one, then long-range interactions occurring in the material micro-structure have to be accounted for, which is not done by classical continuum theory. In such circumstances, molecular/atomistic models do take into account nonlocal

*Correspondence to: Dario De Domenico, Department PAU, University Mediterranea of Reggio Calabria, Reggio Calabria 89124, Italy. Email: dario.dedomenico@unirc.it

interactions between atoms by modelling every single microstructural component individually, nevertheless such models are often computationally prohibitive or extremely demanding on memory resources and thus unfeasible to cope with real engineering problems.

To bridge the gap between atomistic models and classical continuum mechanics theory, a variety of theories and approaches have been studied as extensions of the classical continuum mechanics for applications in microscopic space and time scale, e.g. Cosserat-like continuum theories [27] (including theories of elasticity with couple stress, microcontinuum field theories, micromorphic theory, micropolar elasticity), Mindlin microstructural theory [30], strongly nonlocal Eringen theory [19, 22, 32], weakly nonlocal strain gradient theory [1], and peridynamic theory [35]. A comprehensive review on generalised continuum mechanics theories can be found in [2, 8, 13, 27]. Microstructural enrichment is achieved via the introduction of internal length- and time-scales into an enriched continuum formulation or, alternatively, by equipping the material point with additional degrees of freedom.

In the present paper, attention is focused on gradient elasticity theories. Gradient elasticity models are a special class of the above generalised theories [1, 8]; these models provide extensions of classical elasticity theories in that additional higher-order spatial derivatives of strains, stresses and/or accelerations are considered in the constitutive equations or in the equations of motion. A mathematically complete set of higher-order gradients would be possible, cf. Mindlin [30], but it has been found that a more limited set of higher-order gradients is often sufficient to capture the physical phenomena in most practical engineering problems.

1.1. Goal and outline of the paper

In this paper, a new multi-scale gradient elasticity model is presented that can be used to describe improved dispersion behaviour. This new model contains *three* gradient contributions, namely two micro-inertia terms (acceleration gradients) and one higher-order stiffness term (strain gradient). In the framework of gradient elasticity, the *simultaneous* presence of both acceleration and strain gradients has been denoted as *dynamic consistency* in certain previous articles [5, 8–10, 28, 29]. Dynamically consistent models have been proven to be effective for the removal of singularities [8], as well as for the prediction of dispersive wave propagation [9]. The analytical aspects of a few relevant formats of gradient elasticity are summarised in Section 2. It has been demonstrated that the dispersive capabilities of the dynamically consistent models are better than those of the strain gradient theories: due to the presence of both acceleration and strain gradients, infinite or imaginary phase velocities are avoided altogether [5, 8]. These aspects and the dispersive properties of a class of gradient elasticity models are outlined in Section 3, which motivates a new multi-scale gradient elasticity model as illustrated in Section 4. The present model, in fact, represents an extension of an earlier dynamically consistent model presented in [9] that had only two material parameters (identified as two independent length scales associated to the higher-order inertia term and the higher-order stiffness term). Therefore, similarly to the previous dynamically consistent model, the proposed model can be seen as an enhanced dynamic extension of the strain-gradient elasticity theory developed by Aifantis and coworkers [1, 2, 33]. The resulting formulation incorporates the previous dynamically consistent model as a special case and reduces to the well-known Aifantis' 1992 strain-gradient theory in the quasi-static limit. Compared to the previous dynamically consistent model [9] with two gradient terms, the introduction of an additional micro-inertia term is found to significantly improve the prediction of wave dispersion but requires *no extra computational cost*.

Attention is then focused on how to apply the new model to solve boundary value problems. Due to the fourth-order spatial derivatives entering the equations of motion (both in the inertia-related additional contribution and in the higher-order stiffness term), spatial discretisation would require $\mathscr{C}^1$-continuity of the interpolation, i.e. continuity of the displacements as well as the much more complicated continuity of the displacement derivatives. The fourth-order governing equations are rewritten into two sets of (coupled and symmetric) second-order equations. The related mathematical manipulations are discussed in Section 5. The symmetric format of the split second-order governing equations facilitates the identification of the corresponding kinetic and potential

DOI: 10.1002/nme

energy densities, which is illustrated in Section 6. Positive-definitiveness of the energy functionals is discussed and is related to the relative magnitude of the three material length scale parameters; then, variationally consistent boundary conditions are derived by making use of the Hamilton-Ostrogradsky principle, and the corresponding discretised system of equations are presented in Section 7.

In the coupled second-order equations, two sets of unknowns are identified as the displacements at the *macroscale* and at the *microscale*. The simultaneous appearance of macroscopic and microscopic displacements highlights the multi-scale nature of the present formulation, similarly to Mindlin's theory of elasticity with microstructure. The three higher-order terms are accompanied by three non-standard material parameters that can be calibrated according to the problem being studied. To this aim, in Section 8 two numerical examples are studied and a physically meaningful choice of the material parameters is discussed. More specifically, we present procedures to link the three constitutive coefficients to micro-structural properties. As regards the simulation of wave dispersion, notable improvements of the present formulation over the previous gradient models are observed in the investigated problems. Finally, conclusions are drawn in Section 9.

Notation

Throughout the paper, index tensor notation is used except for Section 7 for finite element discretisation where the more compact matrix-vector notation is adopted. Subscripts denote components with respect to an orthogonal Cartesian coordinate system, say x_i $(i = 1, 2, 3)$; the Einstein summation convention for repeated indices holds. Spatial derivatives are denoted by the comma notation, that is $u_{i,j} = \partial u_i/\partial x_j$ (however, primes are adopted for derivatives with respect to the spatial coordinate x in many instructive discussions related to simple one-dimensional models, that is $u' = \partial u/\partial x$). A super-imposed dot denotes a material time derivative, that is $\dot{u}_i = \partial u_i/\partial t$. The symbol $:=$ means equality by definition. In Section 7 where matrix-vector notation is employed, ∇ denotes the gradient operator, that is, $\nabla = (\partial/\partial x_j)$, and $\nabla^2 = \nabla^T\nabla$ is the Laplace operator. Other symbols will be defined in the text at their first appearance.

2. DIFFERENT FORMATS OF GRADIENT ELASTICITY THEORIES

In principle, different formats of gradient elasticity theories may be studied depending on the number of higher order terms considered in the energy functionals, namely in the potential energy and in the kinetic energy. In this regard and in the spirit of Mindlin's 1964 theory of linear elasticity with microstructure, a general expression of the potential energy density and the kinetic energy density that is of interest for this paper may be written as [8]

$$\mathscr{U}^{\text{pot}} = \frac{1}{2}\varepsilon_{ij}C_{ijkl}\varepsilon_{kl} + \mathscr{H}^{\text{pot}}(\varepsilon_{kl,n}; \varepsilon_{kl,mn}; \ldots) \tag{1a}$$

$$\mathscr{U}^{\text{kin}} = \frac{1}{2}\rho\dot{u}_i\dot{u}_i + \mathscr{H}^{\text{kin}}(\dot{u}_{i,n}; \dot{u}_{i,mn}; \ldots) \tag{1b}$$

where C_{ijkl} is a fourth-order tensor representing the material stiffness, $\varepsilon_{ij} = \frac{1}{2}(u_{i,j} + u_{j,i})$ is the usual strain tensor defined as the symmetric gradient of the displacement field u_i, ρ is the mass density and $\dot{u}_i$ represents the velocity field. In the sequel we will restrict our attention to isotropic materials for which $C_{ijkl} = \lambda\delta_{ij}\delta_{kl} + \mu\delta_{ik}\delta_{jl} + \mu\delta_{il}\delta_{jk}$, δ_{ij} being Kronecker's delta and λ, μ the Lamé constants. In Eqs. (1) the higher-order functionals $\mathscr{H}^{\text{pot}}$ and $\mathscr{H}^{\text{kin}}$ represent the microscale contributions to the potential and kinetic energy density, respectively. These two higher-order contributions are assumed to depend on the gradients of the strain and velocity field.

Two classes of enrichments are therefore possible through the incorporation of higher order gradients of the strain field into expression (1a) and/or higher order gradients of the velocity field into expression (1b). The model dealt with in this paper includes the first-order gradient of the strain field in the potential energy (1a) in addition to the first and second order gradient of the velocity field in the kinetic energy (1b).

DOI: 10.1002/nme

2.1. Aifantis' 1992 strain gradient theory for statics

One of the simplest and most popular theories of gradient elasticity with strain gradients only was developed by Aifantis and coworkers in the mid 1980s [1, 2, 33, 36]. In these articles *one* additional parameter (proportional to the first gradient of the strain field $\varepsilon_{kl,n}$) is introduced in the potential energy (1a) motivated by earlier studies in gradient plasticity and hyperelasticity to describe localized deformation zones. By extending the potential energy with the aforementioned additional parameter, the Laplacian of the strain field appears in the linear elastic constitutive relations, and the associated equilibrium equations $\sigma_{ij,j} + b_i = 0$ in terms of displacements (in the hypothesis of constant stiffness tensor, i.e. homogeneous material) read

$$C_{ijkl}\Big(u_{k,jl} - \ell^2 u_{k,jlnn}\Big) + b_i = 0 \tag{2}$$

where b_i are the body forces and ℓ is a length scale characterising the underlying material microstructure. Indeed, the new parameter ℓ can be linked to microstructural properties—see [8] for an overview. Since the additional energy contribution to $\mathscr{U}^{\text{pot}}$ is positive-definite, uniqueness and stability of the model given in Eq. (2) are guaranteed. This model has successfully been applied to a range of boundary value problems, see e.g. [7, 8] for just a few examples.

As pointed out in [5], the model of Eq. (2) was developed for use in statics: it has gained popularity and has extensively and effectively been used to remove strain singularities that appear at crack tips [1, 2] and dislocation cores [24, 25] as well as to simulate the occurrence of size effects [7, 8]. As will be clarified in Section 3, its straightforward use in dynamics may lead to infinite phase velocities, which is not realistic [5].

2.2. Extension to dynamics: dynamically consistent models

As introduced above, the model of Eq. (2) was developed for applications in statics and its use in dynamics is not recommended as explained in Section 3. As an alternative, a different format of gradient elasticity theories for use in dynamics incorporates mixed spatial-temporal derivatives, that is, higher-order inertia contributions are considered in addition to strain gradient terms.

In order to present a class of such possible extensions of Eq. (2) for use in dynamics, we introduce a general model that incorporates Eq. (2) as special case in the quasi-static limit. This general model is obtained by adding some higher-order terms to the kinetic energy density $\mathscr{U}^{\text{kin}}$, so introducing some higher-order inertia contributions in the equations of motion, while keeping the same format for the potential energy density $\mathscr{U}^{\text{pot}}$ and, thus, for the stiffness (strain-related) contribution. The equations of motion of this model in the hypothesis of homogeneous material (constant density and stiffness tensor) read

$$\rho\Big(\ddot{u}_i - \alpha\ell^2\ddot{u}_{i,nn} + \beta\ell^4\ddot{u}_{i,nnjj}\Big) = C_{ijkl}\Big(u_{k,jl} - \gamma\ell^2 u_{k,jlnn}\Big). \tag{3}$$

The model of Eq. (3) stems from considering additional higher-order contributions to the kinetic energy density as expressed in Eq. (1b). These particular contributions are chosen proportional to the first and second gradient of the velocity field in $\mathscr{U}^{\text{kin}}$.

In Eq. (3) α, β, γ are three coefficients to be calibrated according to the problem being studied. These coefficients *adjust* the relative magnitudes between the various length scales appearing in the strain gradient term and in the micro-inertia contributions. For instance, $\gamma\ell^2$ represents the length scale entering the one-parameter Aifantis' 1992 gradient elasticity theory described above, cf. Eq. (2). Therefore, it can be stated that the model (3) has *three* independent parameters that are three length scales representing the underlying material microstructure. Note that Eq. (2) is retrieved from Eq. (3) if the inertia terms are ignored. Higher-order inertia terms have been motivated by many researchers, see e.g. [1,3,4,17,21]. However, the peculiarity of Eq. (3) is that the higher-order contributions appear *simultaneously* in the stiffness and in the inertia. This fact has been denoted as *dynamic consistency* in a few previous articles, see e.g. [5, 8–10, 28]. Dynamically consistent models have been seen to be effective when applied to statics, for the removal of singularities in the elastic fields [8], as well as to dynamics, for the prediction of dispersive wave propagation [9].

DOI: 10.1002/nme

A dynamically consistent model that is closely related to Eq. (3) has been studied in [9] with two internal parameters, identified as two independent length scales in statics and dynamics, l_s and l_m, respectively. By comparing the format of the dynamically consistent model given in [9] with that of Eq. (3), these two length scales may easily be recognised as $l_m^2 \equiv \alpha\ell^2$ and $l_s^2 \equiv \gamma\ell^2$. Therefore, the dynamically consistent model described by Eq. (3) and developed in this paper represents an extensions of the one developed in [5, 9] with an additional higher-order inertia term (the β micro-inertia contribution) to improve the prediction of wave dispersion as well as to allow for greater flexibility in terms of shape of the corresponding dispersion curve—see Section 3.

Remark 1
An even more complex model may be considered by taking into account a contribution that is proportional to the second-order spatial derivative of the strain in the expression of the potential energy density $\mathscr{U}^{\text{pot}}$, as expressed by the term $\varepsilon_{kl,mn}$ in Eq. (1a). This would result in a sixth-order spatial derivative of the displacements in the right-hand side of the corresponding equations of motion as shown below

$$\rho\Big(\ddot{u}_i - \alpha\ell^2\ddot{u}_{i,nn} + \beta\ell^4\ddot{u}_{i,nnjj}\Big) = C_{ijkl}\Big(u_{k,jl} - \gamma\ell^2 u_{k,jlnn} + \delta\ell^4 u_{k,jlnnkk}\Big) \tag{4}$$

where an additional higher-order strain gradient δ term appears besides the γ term so that both stiffness and inertia include terms of order ℓ^2 as well as ℓ^4. As noted in [5], this would severely complicate the formulation in terms of additional boundary conditions and finite element implementation. Since the aim of this paper is to propose a simple $\mathscr{C}^0$ formulation, we will not take into account this term and we will restrict our attention to the enhanced gradient elasticity model as given by Eq. (3).

3. DISPERSION ANALYSIS OF GRADIENT ELASTICITY MODELS

The main motivation for using gradient elasticity in dynamics has been the simulation of dispersive wave propagation occurring in heterogeneous media. Therefore, with reference to the model expressed by Eq. (3) it is worth reviewing the dispersive behaviour of this model and the relevance, for dynamic applications, of a few special cases that may be retrieved from this particular format of gradient elasticity theories. The signs entering the higher-order coefficients in Eq. (3) are chosen such that the dispersive behaviour of the model is *stable*, i.e. the corresponding phase velocities are real for all wave numbers.

For simplicity, we consider the one-dimensional format of the equation of motion as given in Eq. (3), which reads

$$\rho\ddot{u} - \rho\alpha\ell^2\ddot{u}'' + \rho\beta\ell^4\ddot{u}'''' = Eu'' - E\gamma\ell^2 u'''' \tag{5}$$

where E is the Young's modulus. Since ρ and E are assumed to be constant coefficients, Eq. (5) admits solutions given by a general harmonic function

$$u(x,t) = U\exp(\mathrm{i}(kx - \omega t)) \tag{6}$$

where U is the amplitude, i the imaginary unit, k the wave number and ω the angular frequency. Substituting this solution (6) into the one-dimensional equation of motion (5) yields

$$\rho\,\omega^2 + \rho\alpha\ell^2k^2\omega^2 + \rho\beta\ell^4k^4\omega^2 = Ek^2 + E\gamma\ell^2k^4 \tag{7}$$

that can be rewritten in dimensionless form by introducing the dimensionless wave number $\chi := k\ell$

$$\left(\frac{\omega\ell}{c_e}\right)^2 = \chi^2\,\frac{1+\gamma\chi^2}{1+\alpha\chi^2+\beta\chi^4} \tag{8}$$

where $c_e = \sqrt{E/\rho}$ is the one-dimensional bar velocity of classical elasticity. It can be observed that for the long wavelength limit, i.e. $\chi \to 0$, the phase velocity $c \to c_e$ irrespective of the relative

DOI: 10.1002/nme

magnitudes between the three length scale parameters. Since we are assuming that α, β, γ are positive coefficients, Eq. (8) leads to phase velocities that are real for all the wave numbers χ, in line with the previous remark about the sign of the higher-order terms entering Eq. (3). Moreover, the phase velocity c is also bounded by the elastic bar velocity c_e if one postulates that $\alpha > \gamma$, a fact that has already been observed in [9] for an earlier dynamically consistent model. In the latter paper, this relation between α and γ was also motivated by different arguments concerning the positive-definitiveness of the associated kinetic energy functional, see again [9].

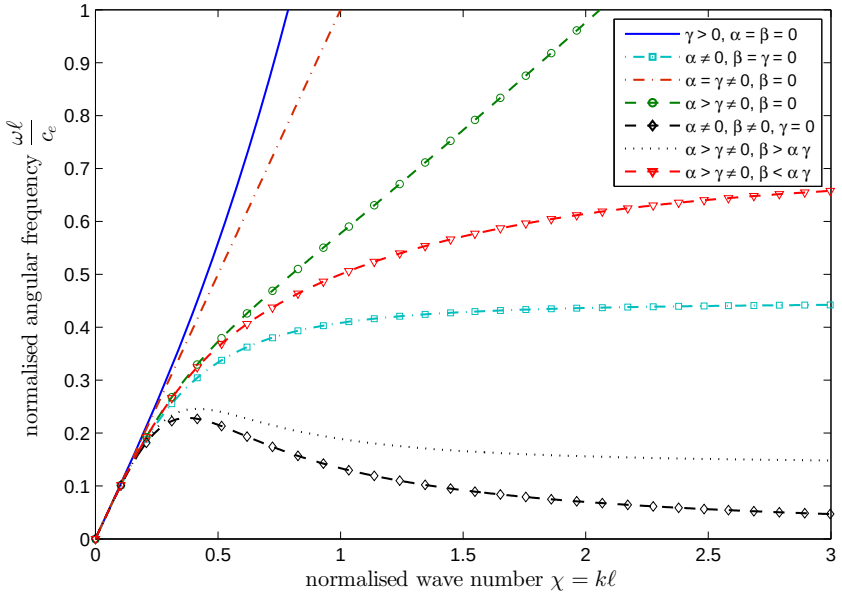

Figure 1. Dispersion properties of the general class of gradient elasticity models given in Eq. (3)—normalised angular frequency *versus* normalised wave number

A few special cases of model (3) may be considered concerning its dispersive behaviour as expressed in Eq. (8). These cases are illustrated in Fig. 1 in terms of dispersion curve $\omega = \omega(\chi)$ (for $\ell = 1$). The curves are obtained for a particular choice of the relative magnitude between the three parameters, namely $\alpha = 5$, $\gamma = 1$ and two values of β, a value of $\beta = 50$ to describe the case in which $\beta > \alpha\gamma$ and $\beta = 2$ to illustrate the dispersive behaviour for the case $\beta < \alpha\gamma$. These cases are summarised as follows:

(i) $\gamma > 0$, $\alpha = \beta = 0$: model (3) reduces to Aifantis' 1992 strain gradient theory developed for statics, Eq. (2). Although the model is dynamically stable, the stable strain gradient leads to frequencies that are larger than those of classical elasticity, which contradicts most experimental evidence. This is why this formulation has been extensively used for statics and not for dynamics;

(ii) $\alpha \neq 0$, $\beta = \gamma = 0$: Eq. (3) yields a so-called 'stable acceleration gradient' model associated with a positive definite kinetic energy density. In this case the dispersion curve $\omega = \omega(\chi)$ is monotonically increasing, has a negative curvature and for $\chi \to \infty$ approaches a horizontal asymptote at angular frequency $1/\sqrt{\alpha}$;

(iii) $\alpha \neq 0$, $\gamma \neq 0$, $\beta = 0$: Eq. (3) leads to the dynamically consistent model as presented in [9]. The dispersion curve shows a diagonal asymptote, the slope of which is governed by the ratio γ/α; therefore, the case $\alpha = \gamma$ leads to a non-dispersive medium (for which the dispersion curve is a straight line given by $\omega = c_e k$). The case $\gamma > \alpha$ means that the higher wave numbers travel faster than the lower wave numbers, which is not realistic as compared to a discrete lattice or to several experiments performed on a range of engineering materials [34,37,39–41],

DOI: 10.1002/nme

the case $\alpha > \gamma$ results in a realistic behaviour in terms of phase velocities and angular frequency, in that the higher wave numbers travel slower than the lower wave numbers;

(iv) $\alpha \neq 0$, $\beta \neq 0$, $\gamma = 0$: this particular format of (3) describes a model with two micro-inertia contributions to capture wave dispersion more accurately than the 'stable acceleration gradient' model as described in (ii). The dispersion curve shows an inflexion (change of curvature), with a peak attained at $\chi = 1/\sqrt[4]{\beta}$, and tends to zero for infinitely large wave numbers.

(v) $\alpha \neq 0$, $\beta \neq 0$, $\gamma \neq 0$: the complete version of model (3) represents an enhanced dynamically consistent model similar to that described in (iii) but with an additional micro-inertia term to improve the dispersion behaviour. If we assume that $\alpha > \gamma > 0$ as suggested in (iii), then if $\beta > \alpha\gamma$ the dispersion curve shows an inflexion like case (iv), with a peak attained at

$$\chi = \sqrt{\frac{\gamma + \sqrt{\gamma^2 + \beta - \alpha\gamma}}{\beta - \alpha\gamma}}, \tag{9}$$

whereas for $\beta < \alpha\gamma$ a monotonically increasing dispersion curve with negative curvature is obtained. In either case, the dispersion curve tends to $\sqrt{\gamma/\beta}$ for infinitely large wave numbers. Note that unlike case (iii), the case $\alpha = \gamma$ does not result in a non-dispersive medium due to the presence of the β term in the denominator of Eq. (8).

We can classify this particular class of gradient elasticity models according to the number of parameters entering the constitutive relations: cases (i) and (ii) are one-parameter gradient elasticity models, cases (iii) and (iv) comprise possible choices of two-parameter models, whereas case (v) represents a more versatile three-parameter gradient elasticity model. Therefore, formulation and finite element implementation of the model given by case (v) would implicitly include the other models as special cases. This is the main aim of the present paper.

4. MOTIVATIONS FOR AN ENHANCED DYNAMICALLY CONSISTENT GRADIENT ELASTICITY MODEL

On the basis of the dispersive properties of the general model given in Eq. (3), it has been found that the inclusion of three free parameters in a gradient elasticity formulation enables a very flexible dispersion curve that can be tailored for a broad variety of engineering materials. It is worth noting that many real engineering materials, see e.g. [37, 39–41], do exhibit a change in the curvature of the $\omega(k)$ curve as predicted by Eq. (8) for non-zero α, β, γ coefficients and for $\beta > \alpha\gamma$, cf. Fig. 1. The presence of the γ term allows for a horizontal asymptote at non-zero angular frequency for large wave numbers, which is confirmed by experimental findings on phonons for a number of engineering materials, see again [37, 39–41]. As an example, in Fig. 2 the experimental dispersion curve of aluminium for phonons propagating in the longitudinal direction is depicted (after Yarnel et al. [41]). Therefore, in order to achieve a qualitative match between numerical and experimental results in terms of dispersive wave propagation, it is of interest to investigate the three parameter gradient elasticity model with α, β and γ different from zero.

As said above, a dynamically consistent model with one higher-order inertia contribution (related to the α term of Eq. (3)) and one strain gradient contribution (related to the γ term of Eq. (3)) has already been investigated and a finite element implementation with $\mathscr{C}^0$-continuous shape functions has effectively been set up [5,8,9,11,15]. In this paper we will show that, according to the comments of the previous Section, the inclusion of another micro-inertia contribution (the β term) significantly improves the dispersion behaviour of the latter model and we will propose a formulation in which such additional term does not imply any extra additional cost from a computational point of view (i.e. with regard to the spatial discretisation and the resulting finite element implementation). The proposed formulation may therefore be considered as an enhanced version of the earlier dynamically consistent model, the latter being retrieved for a zero value of the β term.

DOI: 10.1002/nme

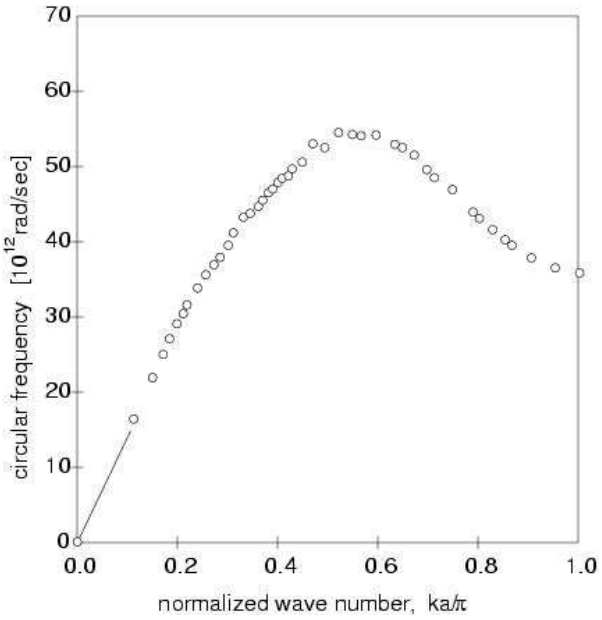

Figure 2. Experimental dispersion curve of aluminium for phonons propagating in the (longitudinal) crystallographic direction [110] (after Yarnel et al. [41])

5. OPERATOR SPLIT

By inspection of Eq. (3) it emerges that fourth-order governing differential equations in the u_i unknowns have to be solved. Solving these fourth-order equations analytically can be an intricate task. Furthermore, if numerical simulations are to be carried out with gradient models, an important aspect concerns the requirements imposed on the discretisation. Formulations of gradient theories that lend themselves to straightforward numerical implementation (e.g. with $\mathscr{C}^0$ finite element methods) are very welcome in this context and are therefore pursued in the present paper. Due to the presence of fourth-order spatial derivatives in Eq. (3), the governing equations would require shape functions that are $\mathscr{C}^1$-continuous. This requirement is not impossible to meet, for example by using Hermitian $\mathscr{C}^1$ finite elements [43], discontinuous Galerkin methods [18], meshless methods [10] or, alternatively, by discretising multiple fields, for instance the displacements and the micro-deformations [42]. Without any criticism of these alternative approaches, an attractive feature of the gradient elasticity model as given in Eq. (3) is related to the possibility to recast the fourth-order differential equations, via a proper operator split, into a set of second-order differential equations so that a standard finite element implementation with $\mathscr{C}^0$-continuous interpolation functions suffices.

For the sake of clarity, we rewrite here the equations of motion as given by Eq. (3) in which we highlight the multi-scale nature of the formulation. Since the equation of motion of the higher-order model are expressed in terms of macroscopic variables, we append a superscript M to the displacements as follows

$$\rho\Big(\ddot{u}_i^M - \alpha\ell^2\ddot{u}_{i,nn}^M + \beta\ell^4\ddot{u}_{i,nnjj}^M\Big) = C_{ijkl}\Big(u_{k,jl}^M - \gamma\ell^2 u_{k,jlnn}^M\Big). \tag{10}$$

We will next rewrite the fourth-order equations of motion expressed by Eq. (10) so that only second-order spatial derivatives of the displacements appear. We consider an auxiliary displacement field u_i^m that is related to the underlying material microstructure and therefore denoted with a superscript m and we eliminate the fourth-order spatial derivative from the right-hand side of Eq. (10) as follows

DOI: 10.1002/nme

$$\rho\Big(\ddot{u}_i^M - \alpha\ell^2\ddot{u}_{i,nn}^M + \beta\ell^4\ddot{u}_{i,nnjj}^M\Big) = C_{ijkl}\,u_{k,jl}^m \tag{11a}$$

$$u_i^M - \gamma\ell^2 u_{i,nn}^M = u_i^m \tag{11b}$$

A justification of the terminology 'microscopic displacements' and 'macroscopic displacements' for the variables u_i^m and u_i^M has been given in [15, 31].

It can be demonstrated that Eqs. (11) can be recast into the following *symmetric* formulation (see Appendix B for the mathematical manipulations involved)

$$\rho\left[\left(\frac{\alpha}{\gamma} - \frac{\beta}{\gamma^2}\right)\ddot{u}_i^m - \frac{\beta\ell^2}{\gamma}\ddot{u}_{i,nn}^m - \left(\frac{\alpha}{\gamma} - \frac{\beta}{\gamma^2} - 1\right)\ddot{u}_i^M\right] = C_{ijkl}\,u_{k,jl}^m \tag{12a}$$

$$\rho\left[-\left(\frac{\alpha}{\gamma} - \frac{\beta}{\gamma^2} - 1\right)\ddot{u}_i^m + \left(\frac{\alpha}{\gamma} - \frac{\beta}{\gamma^2} - 1\right)\ddot{u}_i^M - \left(\alpha - \frac{\beta}{\gamma} - \gamma\right)\ell^2\ddot{u}_{i,nn}^M\right] = 0\,. \tag{12b}$$

The main peculiarity of this format of operator split is that a *fully coupled* set of second-order equations are obtained in which both macroscopic and microscopic displacements appear in the split Eqs. (12). Since both equations are second-order in space, a standard $\mathscr{C}^0$ finite element implementation can be used, which is illustrated in Section 7. Due to the symmetric format of Eqs. (12) (i.e. the coefficient multiplying $\ddot{u}_i^M$ in the first equation is equal to the coefficient multiplying $\ddot{u}_i^m$ in the second equation), the corresponding finite element implementation will lead to symmetric system matrices.

Remark 2
The second-order equations of motion given in Eqs. (12) are an extension of those derived in [9] for a two-parameter dynamically consistent gradient elasticity model. In fact, the latter model is retrieved for the limit case $\beta = 0$.

6. ENERGY FUNCTIONALS AND BOUNDARY CONDITIONS

In order to study the dynamic response of the above developed higher-order model, boundary conditions have to be formulated. To this aim, energy functionals will be identified and used to derive boundary conditions that are variationally consistent with the equations of motion given by Eqs. (12). The Hamilton-Ostrogradsky variational principle is applied by considering the Lagrangian density $\mathscr{L} = \mathscr{U}^{\text{kin}} - \mathscr{U}^{\text{pot}}$, where $\mathscr{U}^{\text{kin}}$ and $\mathscr{U}^{\text{pot}}$ are the kinetic and potential energy densities of the higher-order continuum, respectively. The symmetric format of Eqs. (12) facilitates the identification of such functionals, which can be expressed as

$$\mathscr{U}^{\text{kin}} = \frac{1}{2}\rho\Big[\dot{u}_i^m + \left(\frac{\alpha}{\gamma} - \frac{\beta}{\gamma^2} - 1\right)(\dot{u}_i^m - \dot{u}_i^M)^2 + \frac{\beta\ell^2}{\gamma}(\dot{u}_{i,n}^m)^2 + \left(\alpha - \frac{\beta}{\gamma} - \gamma\right)\ell^2(\dot{u}_{i,n}^M)^2\Big] \tag{13}$$

and

$$\mathscr{U}^{\text{pot}} = \frac{1}{2}\varepsilon_{ij}^m C_{ijkl}\varepsilon_{kl}^m \tag{14}$$

where ε_{ij}^m is the microscopic strain field related to the microscopic displacement field u_i^m. From Eqs. (13) and (14) one may observe that both energy densities are positive definite provided that $\alpha > \frac{\beta}{\gamma} + \gamma$. For the limit case $\beta = 0$ the positive definitiveness of the kinetic energy is guaranteed provided that the condition $\alpha > \gamma$ holds true, see [9].

The Lagrangian function of the body $\mathcal{L}$ is expressed as the integral over the volume of the body of the Lagrangian density $\mathscr{L}$, that is $\mathcal{L} = \int_\Omega \mathscr{L}\,\mathrm{d}\Omega$. Hamilton's principle [38] states that the true evolution of the body Ω between two specified time instants t_1 and t_2 (assumed to be fixed) is a stationary point (with a zero variation) of the following functional, denoted as *action functional*

$$\mathcal{S} = \int_{t_1}^{t_2} \mathcal{L}\,\mathrm{d}t = \int_{t_1}^{t_2}\left(\int_\Omega \mathscr{L}\,\mathrm{d}\Omega\right)\mathrm{d}t. \tag{15}$$

DOI: 10.1002/nme

While in a standard continuum the Lagrangian density is assumed to be a function of the space and time coordinates x_i and t, the displacement field u_i and the *first* derivatives of the displacements with respect to x and t, in a higher-order continuum such as the one developed in this paper higher-order derivatives appear in $\mathscr{L}$, i.e. mixed time-space derivatives as well as higher-order spatial derivatives.

After applying the operator split described in the Section 5, the coupled second-order equations of motion (12) are obtained that are expressed in terms of both macroscopic and microscopic displacements, u_i^M and u_i^m, respectively. The Lagrangian density for this second-order model is a function of variables at both macroscopic and microscopic scale of observation and can be expressed as follows

$$\mathscr{L} = \mathscr{L}\big(x_i, t, \dot{u}_i^m, \dot{u}_{i,n}^m, u_{i,n}^m, \dot{u}_i^M, \dot{u}_{i,n}^M\big). \tag{16}$$

We denote with $u_i^M(x_i,t)$ and $u_i^m(x_i,t)$ the displacement fields describing the motion of the body from instant t_1 until instant t_2 or, equivalently, representing a stationary point for the action functional $\mathcal{S}$ given in Eq. (15). We can consider slightly perturbed displacements fields in the following form

$$\tilde{u}_i^m(x_i,t) = u_i^m(x_i,t) + e\,\xi_i(x_i,t) \tag{17a}$$
$$\tilde{u}_i^M(x_i,t) = u_i^M(x_i,t) + e\,\eta_i(x_i,t) \tag{17b}$$

where e is the amplitude of the perturbation and $\xi_i(x_i,t)$ and $\eta_i(x_i,t)$ are two normalised perturbation fields. Since $\tilde{u}_i^m(x_i,t)$ and $\tilde{u}_i^M(x_i,t)$ also describe the motion of the body from t_1 to t_2, the conditions $\xi_i(x_i,t_1) = \xi_i(x_i,t_2) = 0$ and $\eta_i(x_i,t_1) = \eta_i(x_i,t_2) = 0$ hold true. For the same reasons, also their spatial derivatives should vanish at the limits of the time interval.

Hamilton's stationary principle (15) applied to the perturbed displacement fields (17) requires that

$$\frac{\mathrm{d}}{\mathrm{d}e}\left(\int_{t_1}^{t_2}\int_\Omega \mathscr{L}\,\mathrm{d}\Omega\,\mathrm{d}t\right)\bigg|_{e=0} = 0 \tag{18}$$

By taking into account the general expression of the Lagrangian density $\mathscr{L}$ as given in (16) and separating terms in microscopic and macroscopic displacements, Eq. (18) can be elaborated as the following two equations

$$\int_{t_1}^{t_2}\int_\Omega \left(\frac{\partial\mathscr{L}}{\partial\dot{u}_i^m}\dot{\xi}_i + \frac{\partial\mathscr{L}}{\partial\dot{u}_{i,n}^m}\dot{\xi}_{i,n} + \frac{\partial\mathscr{L}}{\partial u_{i,n}^m}\xi_{i,n}\right)\mathrm{d}\Omega\,\mathrm{d}t = 0 \tag{19a}$$
$$\int_{t_1}^{t_2}\int_\Omega \left(\frac{\partial\mathscr{L}}{\partial\dot{u}_i^M}\dot{\eta}_i + \frac{\partial\mathscr{L}}{\partial\dot{u}_{i,n}^M}\dot{\eta}_{i,n}\right)\mathrm{d}\Omega\,\mathrm{d}t = 0 \tag{19b}$$

that represent Eqs. (12) in the Lagrangian form. The aim is now to rewrite Eqs. (19) such that no time or mixed time-space derivatives of ξ_i and η_i appear and in which the contributions of the spatial boundaries are collected, so as to identify essential and natural boundary conditions that are variationally consistent. To this aim, we perform integration by parts which results in

$$\frac{\partial\mathscr{L}}{\partial\dot{u}_i^m}\dot{\xi}_i = -\xi_i\frac{\partial}{\partial t}\frac{\partial\mathscr{L}}{\partial\dot{u}_i^m} + \frac{\partial}{\partial t}\left(\frac{\partial\mathscr{L}}{\partial\dot{u}_i^m}\xi_i\right) \tag{20a}$$
$$\begin{aligned}\frac{\partial\mathscr{L}}{\partial\dot{u}_{i,n}^m}\dot{\xi}_{i,n} &= -\xi_{i,n}\frac{\partial}{\partial t}\frac{\partial\mathscr{L}}{\partial\dot{u}_{i,n}^m} + \frac{\partial}{\partial t}\left(\frac{\partial\mathscr{L}}{\partial\dot{u}_{i,n}^m}\xi_{i,n}\right) = \\ &= \xi_i\frac{\partial^2}{\partial t\,\partial x_n}\frac{\partial\mathscr{L}}{\partial\dot{u}_{i,n}^m} - \frac{\partial}{\partial x_n}\left(\xi_i\frac{\partial}{\partial t}\frac{\partial\mathscr{L}}{\partial\dot{u}_{i,n}^m}\right) + \frac{\partial}{\partial t}\left(\frac{\partial\mathscr{L}}{\partial\dot{u}_{i,n}^m}\xi_{i,n}\right)\end{aligned} \tag{20b}$$
$$\frac{\partial\mathscr{L}}{\partial u_{i,n}^m}\xi_{i,n} = -\xi_i\frac{\partial}{\partial x_n}\frac{\partial\mathscr{L}}{\partial u_{i,n}^m} + \frac{\partial}{\partial x_n}\left(\frac{\partial\mathscr{L}}{\partial u_{i,n}^m}\xi_i\right) \tag{20c}$$

DOI: 10.1002/nme

with reference to Eq. (19a) and, similarly,

$$\frac{\partial \mathscr{L}}{\partial \dot{u}_i^M}\dot{\eta}_i = -\eta_i \frac{\partial}{\partial t}\frac{\partial \mathscr{L}}{\partial \dot{u}_i^M} + \frac{\partial}{\partial t}\left(\frac{\partial \mathscr{L}}{\partial \dot{u}_i^M}\eta_i\right) \tag{21a}$$

$$\frac{\partial \mathscr{L}}{\partial \dot{u}_{i,n}^M}\dot{\eta}_{i,n} = -\eta_{i,n}\frac{\partial}{\partial t}\frac{\partial \mathscr{L}}{\partial \dot{u}_{i,n}^M} + \frac{\partial}{\partial t}\left(\frac{\partial \mathscr{L}}{\partial \dot{u}_{i,n}^M}\eta_{i,n}\right) =$$
$$= \eta_i \frac{\partial^2}{\partial t\,\partial x_n}\frac{\partial \mathscr{L}}{\partial \dot{u}_{i,n}^M} - \frac{\partial}{\partial x_n}\left(\eta_i \frac{\partial}{\partial t}\frac{\partial \mathscr{L}}{\partial \dot{u}_{i,n}^M}\right) + \frac{\partial}{\partial t}\left(\frac{\partial \mathscr{L}}{\partial \dot{u}_{i,n}^N}\eta_{i,n}\right) \tag{21b}$$

with reference to Eq. (19b).

Substituting Eqs. (20) into Eq. (19a) yields

$$\int_\Omega \left(\xi_i \frac{\partial \mathscr{L}}{\partial \dot{u}_i^m} + \xi_{i,n}\frac{\partial \mathscr{L}}{\partial \dot{u}_{i,n}^m}\right)\mathrm{d}\Omega\Big|_{t_1}^{t_2} + \int_{t_1}^{t_2}\oint_\Gamma \xi_i\left(\frac{\partial \mathscr{L}}{\partial u_{i,n}^m} - \frac{\partial}{\partial t}\frac{\partial \mathscr{L}}{\partial \dot{u}_{i,n}^m}\right)n_n \mathrm{d}\Gamma\,\mathrm{d}t$$
$$- \int_{t_1}^{t_2}\int_\Omega \xi_i\left(\frac{\partial}{\partial t}\frac{\partial \mathscr{L}}{\partial \dot{u}_i^m} - \frac{\partial^2}{\partial t\,\partial x_n}\frac{\partial \mathscr{L}}{\partial \dot{u}_{i,n}^m} + \frac{\partial}{\partial x_n}\frac{\partial \mathscr{L}}{\partial u_{i,n}^m}\right)\mathrm{d}\Omega\,\mathrm{d}t = 0 \tag{22}$$

where the divergence theorem has been applied to rewrite the second integral as a surface integral, in which Γ denotes the boundary surface of the volume Ω and n_n is the outward normal to Γ. In a similar manner, substituting Eqs. (21) into Eq. (19b) leads to

$$\int_\Omega \left(\eta_i \frac{\partial \mathscr{L}}{\partial \dot{u}_i^M} + \eta_{i,n}\frac{\partial \mathscr{L}}{\partial \dot{u}_{i,n}^M}\right)\mathrm{d}\Omega\Big|_{t_1}^{t_2} - \int_{t_1}^{t_2}\oint_\Gamma \eta_i\left(\frac{\partial}{\partial t}\frac{\partial \mathscr{L}}{\partial \dot{u}_{i,n}^M}\right)n_n \mathrm{d}\Gamma\,\mathrm{d}t$$
$$- \int_{t_1}^{t_2}\int_\Omega \eta_i\left(\frac{\partial}{\partial t}\frac{\partial \mathscr{L}}{\partial \dot{u}_i^M} - \frac{\partial^2}{\partial t\,\partial x_n}\frac{\partial \mathscr{L}}{\partial \dot{u}_{i,n}^M}\right)\mathrm{d}\Omega\,\mathrm{d}t = 0. \tag{23}$$

From Eqs. (22) and (23) we note that, following the considerations made above, the first integral vanishes as ξ_i, η_i, $\xi_{i,n}$ and $\eta_{i,n}$ are zero at the limits of the time interval. Thus, the sum of the second and third integrals in Eqs. (22) and (23) should vanish. Since this should hold for any arbitrary domain, it is required that each integral vanishes separately [28]. Therefore, from the third integral in (22) and (23) we derive the Lagrangian format of the equations of motion for the developed gradient elasticity model

$$\frac{\partial}{\partial t}\frac{\partial \mathscr{L}}{\partial \dot{u}_i^m} - \frac{\partial^2}{\partial t\,\partial x_n}\frac{\partial \mathscr{L}}{\partial \dot{u}_{i,n}^m} + \frac{\partial}{\partial x_n}\frac{\partial \mathscr{L}}{\partial u_{i,n}^m} = 0 \tag{24a}$$

$$\frac{\partial}{\partial t}\frac{\partial \mathscr{L}}{\partial \dot{u}_i^M} - \frac{\partial^2}{\partial t\,\partial x_n}\frac{\partial \mathscr{L}}{\partial \dot{u}_{i,n}^M} = 0. \tag{24b}$$

It can easily be verified that these conditions are fulfilled by the Lagrangian density $\mathscr{L} = \mathscr{U}^{\mathrm{kin}} - \mathscr{U}^{\mathrm{pot}}$, where $\mathscr{U}^{\mathrm{kin}}$ and $\mathscr{U}^{\mathrm{pot}}$ are given in (13) and (14). On the other hand, from the second integral in (22) and (23) we can derive variationally consistent boundary conditions (cf. [28]):

- *essential* boundary conditions are given through prescribed values of

$$u_i^m = \bar{u}_i^m \tag{25a}$$

$$u_i^M = \bar{u}_i^M \tag{25b}$$

  such that $\xi_i = 0$ and $\eta_i = 0$ over the boundary surface;

- *natural* boundary conditions are given through prescribed values of

$$-n_n\left(\frac{\partial \mathscr{L}}{\partial u_{i,n}^m} - \frac{\partial}{\partial t}\frac{\partial \mathscr{L}}{\partial \dot{u}_{i,n}^m}\right) = n_n\left(C_{ijkl}\varepsilon_{kl}^m + \rho\frac{\beta\ell^2}{\gamma}\ddot{u}_{i,n}^m\right) \tag{26a}$$

$$n_n\left(\frac{\partial}{\partial t}\frac{\partial \mathscr{L}}{\partial \dot{u}_{i,n}^M}\right) = n_n\,\rho\left(\alpha - \frac{\beta}{\gamma} - \gamma\right)\ell^2\ddot{u}_{i,n}^M \tag{26b}$$

  such that the second integrals in (22) and (23) vanish when integrated over the time interval.

DOI: 10.1002/nme

7. FINITE ELEMENT IMPLEMENTATION

In this section we will discuss the finite element implementation of Eqs. (12) in the most general 3D case. Since both equations are second-order in space, a standard $\mathscr{C}^0$-continuity of the shape functions is sufficient. Only for this Section we will employ the more compact matrix-vector notation in place of the index tensor notation adopted in the remainder of the paper. For the sake of generality, discretisation of the micro- and macro-displacements $\mathbf{u}^m$ and $\mathbf{u}^M$ is performed with two classes of shape functions N_i^m and N_i^M, respectively, that are collected in two matrices as follows

$$\begin{aligned}\mathbf{N}^m &= \begin{bmatrix} N_1^m & 0 & 0 & N_2^m & 0 & 0 & \dots \\ 0 & N_1^m & 0 & 0 & N_2^m & 0 & \dots \\ 0 & 0 & N_1^m & 0 & 0 & N_2^m & \dots \end{bmatrix} \\ \mathbf{N}^M &= \begin{bmatrix} N_1^M & 0 & 0 & N_2^M & 0 & 0 & \dots \\ 0 & N_1^M & 0 & 0 & N_2^M & 0 & \dots \\ 0 & 0 & N_1^M & 0 & 0 & N_2^M & \dots \end{bmatrix}\end{aligned} \tag{27}$$

The continuum micro- and macro-displacements $\mathbf{u}^m = [u_x^m, u_y^m, u_z^m]^T$ and $\mathbf{u}^M = [u_x^M, u_y^M, u_z^M]^T$ are related to the nodal displacements $\mathbf{d}^m = [d_{1x}^m, d_{1y}^m, d_{1z}^m, d_{2x}^m, d_{2y}^m, d_{2z}^m \dots]$ and $\mathbf{d}^M = [d_{1x}^M, d_{1y}^M, d_{1z}^M, d_{2x}^M, d_{2y}^M, d_{2z}^M, \dots]$ via $\mathbf{u}^m = \mathbf{N}^m\mathbf{d}^m$ and $\mathbf{u}^M = \mathbf{N}^M\mathbf{d}^M$. The coupled set of second-order equations (12) in matrix-vector notation reads

$$\rho\left[\left(\frac{\alpha}{\gamma} - \frac{\beta}{\gamma^2}\right)\ddot{\mathbf{u}}^m - \frac{\beta\ell^2}{\gamma}\nabla^2\ddot{\mathbf{u}}^m - \left(\frac{\alpha}{\gamma} - \frac{\beta}{\gamma^2} - 1\right)\ddot{\mathbf{u}}^M\right] - \mathbf{L}^T\mathbf{C}\mathbf{L}\mathbf{u}^m = 0 \tag{28a}$$

$$\rho\left[-\left(\frac{\alpha}{\gamma} - \frac{\beta}{\gamma^2} - 1\right)\ddot{\mathbf{u}}^m + \left(\frac{\alpha}{\gamma} - \frac{\beta}{\gamma^2} - 1\right)\ddot{\mathbf{u}}^M - \left(\alpha - \frac{\beta}{\gamma} - \gamma\right)\ell^2\nabla^2\ddot{\mathbf{u}}^M\right] = 0 \tag{28b}$$

where the usual differential operators ∇ and $\mathbf{L}$ are employed that in the general 3D case are defined as follows

$$\nabla^T = \begin{bmatrix} \frac{\partial}{\partial x} & \frac{\partial}{\partial y} & \frac{\partial}{\partial z} \end{bmatrix}, \quad \mathbf{L}^T = \begin{bmatrix} \frac{\partial}{\partial x} & 0 & 0 & \frac{\partial}{\partial y} & 0 & \frac{\partial}{\partial z} \\ 0 & \frac{\partial}{\partial y} & 0 & \frac{\partial}{\partial x} & \frac{\partial}{\partial z} & 0 \\ 0 & 0 & \frac{\partial}{\partial z} & 0 & \frac{\partial}{\partial y} & \frac{\partial}{\partial x} \end{bmatrix} \tag{29}$$

such that $\boldsymbol{\varepsilon}^m = \mathbf{L}\mathbf{u}^m$, while $\nabla^2 = \nabla^T \cdot \nabla$ is the Laplace operator. Given two vectors of test functions $\mathbf{w} = [w_x, w_y, w_z]^T$ and $\mathbf{v} = [v_x, v_y, v_z]^T$, we take the the weak form of Eqs. (28)

$$\begin{aligned}&\int_\Omega \mathbf{w}^T\rho\left[\left(\frac{\alpha}{\gamma} - \frac{\beta}{\gamma^2}\right)\ddot{\mathbf{u}}^m - \left(\frac{\alpha}{\gamma} - \frac{\beta}{\gamma^2} - 1\right)\ddot{\mathbf{u}}^M\right]\mathrm{d}\Omega \\ &- \int_\Omega \mathbf{w}^T\rho\,\frac{\beta\ell^2}{\gamma}\nabla^2\ddot{\mathbf{u}}^m\mathrm{d}\Omega - \int_\Omega \mathbf{w}^T\mathbf{L}^T\mathbf{C}\mathbf{L}\mathbf{u}^m\mathrm{d}\Omega = 0\end{aligned} \tag{30a}$$

$$\begin{aligned}&\int_\Omega \mathbf{v}^T\rho\left[-\left(\frac{\alpha}{\gamma} - \frac{\beta}{\gamma^2} - 1\right)\ddot{\mathbf{u}}^m + \left(\frac{\alpha}{\gamma} - \frac{\beta}{\gamma^2} - 1\right)\ddot{\mathbf{u}}^M\right]\mathrm{d}\Omega \\ &- \int_\Omega \mathbf{v}^T\rho\left(\alpha - \frac{\beta}{\gamma} - \gamma\right)\ell^2\nabla^2\ddot{\mathbf{u}}^M\mathrm{d}\Omega = 0.\end{aligned} \tag{30b}$$

DOI: 10.1002/nme

Integrating the last two terms of Eq. (30a) and the last term of Eq. (30b) by parts leads to

$$\int_\Omega \mathbf{w}^T \rho \left[\left(\frac{\alpha}{\gamma} - \frac{\beta}{\gamma^2} \right) \ddot{\mathbf{u}}^m - \left(\frac{\alpha}{\gamma} - \frac{\beta}{\gamma^2} - 1 \right) \ddot{\mathbf{u}}^M \right] \mathrm{d}\Omega$$
$$+ \sum_{\xi=x,y,z} \int_\Omega \frac{\partial \mathbf{w}^T}{\partial \xi} \rho \frac{\beta \ell^2}{\gamma} \frac{\partial \ddot{\mathbf{u}}^m}{\partial \xi} \mathrm{d}\Omega + \int_\Omega \left(\mathbf{L}\mathbf{w} \right)^T \mathbf{C} \mathbf{L} \mathbf{u}^m \mathrm{d}\Omega = \int_{\Gamma_n} \mathbf{w}^T \mathbf{t} \, \mathrm{d}\Gamma \tag{31a}$$

$$\int_\Omega \mathbf{v}^T \rho \left[-\left(\frac{\alpha}{\gamma} - \frac{\beta}{\gamma^2} - 1 \right) \ddot{\mathbf{u}}^m + \left(\frac{\alpha}{\gamma} - \frac{\beta}{\gamma^2} - 1 \right) \ddot{\mathbf{u}}^M \right] \mathrm{d}\Omega$$
$$+ \sum_{\xi=x,y,z} \int_\Omega \frac{\partial \mathbf{v}^T}{\partial \xi} \left(\alpha - \frac{\beta}{\gamma} - \gamma \right) \ell^2 \frac{\partial \ddot{\mathbf{u}}^M}{\partial \xi} \mathrm{d}\Omega = \oint_\Gamma \mathbf{v}^T \rho \left(\alpha - \frac{\beta}{\gamma} - \gamma \right) \ell^2 \left(\mathbf{n} \cdot \nabla \ddot{\mathbf{u}}^M \right) \mathrm{d}\Gamma. \tag{31b}$$

In Eqs. (31) $\mathbf{t} = [t_x, t_y, t_z]^T$ are the user-prescribed tractions on the Neumann part Γ_n that, in line with Eq. (26a), are expressed as $\mathbf{t} = \mathbf{N}^T \left(\mathbf{C}\mathbf{L}\mathbf{u}^m + \rho \frac{\beta \ell^2}{\gamma} \nabla \ddot{\mathbf{u}}^m \right)$, where the matrix $\mathbf{N}$ contains the components of the outward normal vector $\mathbf{n} = [n_x, n_y, n_z]^T$ to the boundary Γ and is arranged similarly to the $\mathbf{L}$ operator reported in (29). Ignoring the boundary integrals related to the inertia terms appearing in the right-hand side of Eq. (31b) and by using the displacement shape functions $\mathbf{N}^m$ and $\mathbf{N}^M$ also for the two test functions, the semi-discretised format of Eqs. (31) (i.e. discretised in space) can be rewritten as

$$\begin{bmatrix} \mathbf{M}_{11} & -\mathbf{M}_{12} \\ -\mathbf{M}_{12}^T & \mathbf{M}_{22} \end{bmatrix} \begin{bmatrix} \ddot{\mathbf{d}}^m \\ \ddot{\mathbf{d}}^M \end{bmatrix} + \begin{bmatrix} \mathbf{K}_{11} & \mathbf{0} \\ \mathbf{0} & \mathbf{0} \end{bmatrix} \begin{bmatrix} \mathbf{d}^m \\ \mathbf{d}^M \end{bmatrix} = \begin{bmatrix} \mathbf{f}_{\text{ext}} \\ \mathbf{0} \end{bmatrix} \tag{32}$$

where

$$\mathbf{M}_{11} = \int_\Omega \mathbf{N}^{mT} \rho \left(\frac{\alpha}{\gamma} - \frac{\beta}{\gamma^2} \right) \mathbf{N}^m \mathrm{d}\Omega + \sum_{\xi=x,y,z} \int_\Omega \frac{\partial \mathbf{N}^{mT}}{\partial \xi} \rho \frac{\beta \ell^2}{\gamma} \frac{\partial \mathbf{N}^m}{\partial \xi} \mathrm{d}\Omega \tag{33a}$$

$$\mathbf{M}_{12} = \int_\Omega \mathbf{N}^{mT} \rho \left(\frac{\alpha}{\gamma} - \frac{\beta}{\gamma^2} - 1 \right) \mathbf{N}^M \mathrm{d}\Omega \tag{33b}$$

$$\mathbf{M}_{22} = \int_\Omega \mathbf{N}^{MT} \rho \left(\frac{\alpha}{\gamma} - \frac{\beta}{\gamma^2} - 1 \right) \mathbf{N}^M \mathrm{d}\Omega + \sum_{\xi=x,y,z} \int_\Omega \frac{\partial \mathbf{N}^{MT}}{\partial \xi} \rho \left(\alpha - \frac{\beta}{\gamma} - \gamma \right) \ell^2 \frac{\partial \mathbf{N}^M}{\partial \xi} \mathrm{d}\Omega \tag{33c}$$

$$\mathbf{K}_{11} = \int_\Omega \mathbf{B}^{mT} \mathbf{C} \mathbf{B}^m \mathrm{d}\Omega \tag{33d}$$

$$\mathbf{f}_{\text{ext}} = \int_{\Gamma_n} \mathbf{N}^{mT} \mathbf{t} \, \mathrm{d}\Gamma \tag{33e}$$

and $\mathbf{B}^m = \mathbf{L}\mathbf{N}^m$. Stability issues of the proposed finite element implementation are discussed in Appendix A. Interestingly, stability of the finite element implementation is guaranteed even if the energy functionals discussed in Section 6 are not positive-definite.

For the time discretisation of Eqs. (32) the unconditionally stable constant average acceleration variant of the Newmark scheme can be used so as to have no restrictions on the time step.

Remark 3

The equations of motion presented in (3) can be derived from a constitutive relation having the following format

$$\sigma_{ij} = C_{ijkl}(\varepsilon_{kl} - \gamma \ell^2 \varepsilon_{kl,nn}) + \rho(\alpha \ell^2 \ddot{u}_{i,j} - \beta \ell^4 \ddot{u}_{i,jkk}) \tag{34}$$

where higher-order contributions appear simultaneously in the stiffness-related and in the inertia-related part. In fact, the two natural boundary conditions appearing in Eqs. (31), consistent with expressions (26), involve two contributions to the stress tensor of the proposed model, i.e. a

Prepared using nmeauth.cls
DOI: 10.1002/nme

'stiffness' contribution

$$\sigma_{ij}^{\mathrm{st}} = C_{ijkl}\varepsilon_{kl}^{m} + \rho\frac{\beta\ell^2}{\gamma}\ddot{u}_{i,n}^{m} = C_{ijkl}\varepsilon_{kl}^{m} + \eta\,\ddot{\varepsilon}_{ij}^{m} \tag{35}$$

consisting of the Hookean stress plus an additional term depending on the β microstructural parameter, and a pure 'inertia' contribution

$$\sigma_{ij}^{\mathrm{in}} = \rho\left(\alpha - \frac{\beta}{\gamma} - \gamma\right)\ell^2\ddot{u}_{i,n}^{M} \tag{36}$$

that is affected by the macroscopic acceleration field. The natural choice has been to set the 'stiffness' traction associated to $\sigma_{ij}^{\mathrm{st}}$ equal to the externally applied traction, and to assume homogeneous natural boundary conditions corresponding to the 'inertia' traction $\sigma_{ij}^{\mathrm{in}}$ (cf. also [8,9]).

Remark 4
Although the operator split applied to the original equations (10) results in a two-field formulation, this is not a reducible form. The reason is that time derivatives have been taken in arriving at Eq. (B1), therefore the original formulation of Eq. (3) can no longer be retrieved. Therefore, the proposed formulation is not a mixed formulation and the restrictions on the interpolation as follow from the Babuška-Brezzi (or inf-sup) condition do not apply. Since the interpolation regards two displacement fields (and not displacement and strain fields, as for example in [6], or displacements and micro-deformations, as in [42]), an obvious choice is to use the same shape functions for both the variables, which is done in all the numerical examples of the paper.

8. NUMERICAL EXAMPLES

In this section, dynamic problems are investigated with the aim to assess the effectiveness and accuracy of the proposed enhanced gradient elasticity formulation in capturing the dispersive wave propagation. For simplicity and brevity, we only focus on one-dimensional problems to validate the developed gradient elasticity formulation by comparison with results given by reference solutions as well as by other formats of gradient elasticity. Multi-dimensional examples as well as additional computational aspects regarding the accuracy of the numerical solution and the optimal choice of the time-step and the element size of the proposed model will be discussed in a follow-up study.

The test set-up is shown in Fig. 3, namely a one-dimensional bar having length L, subjected to a force F at its left hand end and fixed at the opposite right hand end. The length of the bar, direction and time history of the applied force, the material properties as well as the higher-order coefficients characterising the gradient elasticity model are specified for each particular example.

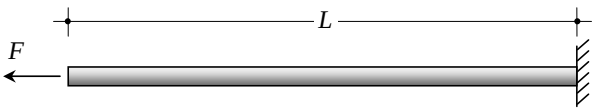

Figure 3. One-dimensional dynamic bar problem: geometry, loading and boundary conditions

With reference to the simple model given in Fig. 3, two physical phenomena are numerically simulated, namely the dispersive wave propagation in a discrete chain of masses and springs and the dispersive wave propagation occurring in a periodically heterogenous composite laminate. A physically meaningful choice of the three material length scale parameters is discussed for these two problems. More specifically, we elaborate procedures to link the three constitutive coefficients to micro-structural properties. We will show that considerable improvements of the present formulation over previous formats of gradient models are observed in the investigated problems, which is due to the additional micro-inertia β contribution in the gradient elasticity formulation.

DOI: 10.1002/nme

8.1. Discrete chain of masses and springs

In many studies, gradient elasticity theories have been derived from the continualisation of the response of a discrete lattice, see e.g. [5, 10, 16, 23, 28, 29]. It is, thus, interesting to investigate to which extent the dynamic behaviour of such discrete lattice can be captured by the proposed gradient elasticity formulation.

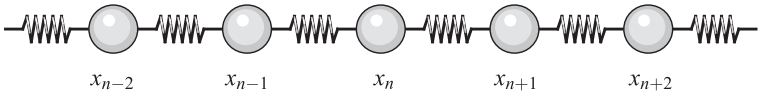

Figure 4. One-dimensional discrete lattice consisting of mass particles connected by springs

We consider the one-dimensional chain of mass particles being connected by springs that is depicted in Fig. 4. All particles have mass M and all springs have stiffness K; furthermore, the particle spacing is denoted with ℓ. The equation of motion for the central particle n is written as

$$M\ddot{u}_n(t) = K\big(u_{n-1}(t) - 2u_n(t) + u_{n+1}(t)\big). \tag{37}$$

where $u_n(t)$ is the displacement of the mass particle n initially located at x_n. Continualisation is performed by translating the response of the discrete particle $u_n(t)$ into the continuous displacement $u(x,t)$. For the neighbouring particles this implies $u_{n\pm1}(t) = u(x \pm \ell, t)$, due to the fact that $x_{n\pm1} = x_n \pm \ell$. The continuous counterpart of the equation of motion given in Eq. (37) is therefore written as

$$\rho A\ell\, \ddot{u}(x,t) = \frac{EA}{\ell}\Big(u(x-\ell,t) - 2u(x,t) + u(x+\ell,t)\Big). \tag{38}$$

where ρ is the mass density, E is the Young's modulus and A is the cross-sectional area. By using Taylor expansions for $u(x-\ell,t)$ and $u(x+\ell,t)$, Eq. (38) can be rewritten as

$$\rho\, \ddot{u}(x,t) = E\Big(u''(x,t) + \frac{1}{12}\ell^2 u''''(x,t) + \frac{1}{360}\ell^4 u''''''(x,t)\Big) + \mathcal{O}(\ell^6). \tag{39}$$

As indicated, Eq. (39) is asymptotically accurate up to $\mathcal{O}(\ell^6)$.

Following the discussion in Section 3 regarding the sign of the higher-order contributions in gradient elasticity models, we note that the positive sign of the $u(x,t)''''$ term is destabilising and would result in loss of uniqueness in boundary value problems and dynamic instability. This term can be replaced by a stable higher-order inertia term as follows: the second space derivative is taken from Eq. (39), the result is multiplied with $\frac{1}{12}\ell^2$ and subtracted from Eq. (39). By omitting, for simplicity, the space and time dependence of the displacement, that is, $u = u(x,t)$, and by ignoring terms beyond or including $\mathcal{O}(\ell^6)$, the mathematical manipulations described above yield

$$\rho\left(\ddot{u} - \frac{1}{12}\ell^2\ddot{u}''\right) = E\Big(u'' - \frac{1}{240}\ell^4 u''''''\Big) + \mathcal{O}(\ell^6). \tag{40}$$

Again, since the negative sign of the u'''''' term is destabilising, cf. Eq. (4), we eliminate this term as follows: the fourth space derivative is taken from Eq. (39), the result is multiplied with $\frac{1}{240}\ell^4$ and added to Eq. (40). Ignoring terms beyond or including $\mathcal{O}(\ell^6)$, the mathematical manipulations described above lead to

$$\rho\left(\ddot{u} - \frac{1}{12}\ell^2\ddot{u}'' + \frac{1}{240}\ell^4\ddot{u}''''\right) = Eu'' + \mathcal{O}(\ell^6). \tag{41}$$

Note that the truncation error of Eqs. (39) and (41) is the same, namely $\mathcal{O}(\ell^6)$, but the latter equation contains only stable terms.

By comparing Eq. (41) obtained via the continualisation procedure of a discrete lattice, and Eq. (5) representing the one-dimensional format of the equation of motion of the proposed enhanced

DOI: 10.1002/nme

gradient elasticity model, the three model parameters α, β and γ are identified for this problem as

$$\alpha = \frac{1}{12}, \quad \beta = \frac{1}{240}, \quad \gamma = 0. \tag{42}$$

Therefore, for the numerical simulation of the dispersive wave propagation occurring in a discrete lattice of masses and springs as depicted in Fig. 4, the length scale parameter ℓ is set equal to the particle spacing, the values of α and β are given in (42) and an infinitely small value of γ should be assumed accordingly.

The prediction of wave dispersion in a discrete chain of masses and springs has already been investigated in [11] by means of two different gradient elasticity models, namely a so-called 'α-model' with a higher-order inertia contribution proportional to $\ddot{u}''$ (obtained by the proposed model for a zero value of the β term) and a so-called 'causal model' in which, in addition to the aforementioned $\ddot{u}''$-term (α term), a contribution proportional to the fourth-order time derivative $\ddddot{u}$ was considered to retain *causality* of the formulation (more details can be found in the quoted paper [11]).

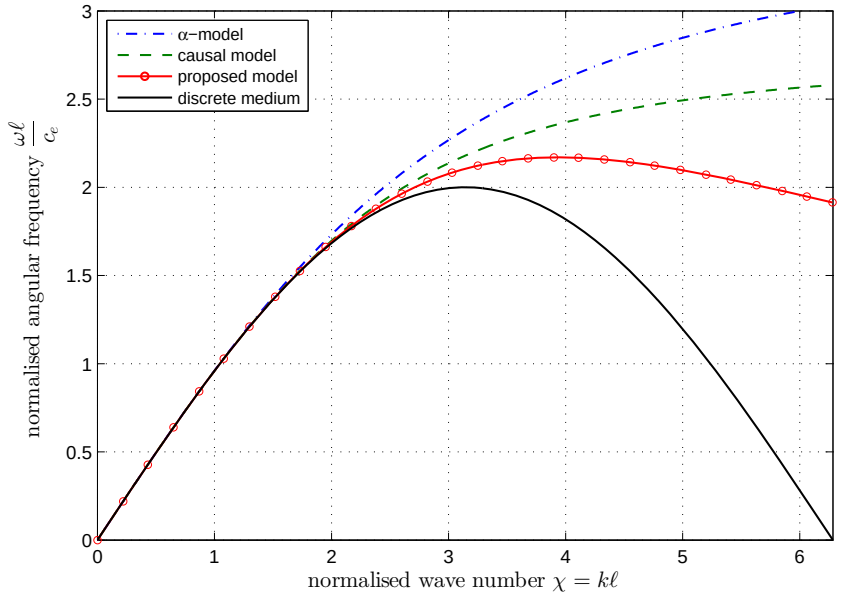

Figure 5. Dispersion properties of three gradient elasticity models compared to the dispersion properties of a discrete chain of masses and springs—normalised angular frequency *versus* normalised wave number

Since we are interested in evaluating the performance of the proposed formulation and the improvements over previous gradient elasticity models, in Fig. 5 the dispersion curves of the three gradient elasticity models are plotted and compared to the reference dispersion curve of the discrete medium. The dispersion curve of the discrete medium may easily be obtained by considering a general harmonic function for the central particle n in the form

$$u_n(x,t) = U \exp(\mathrm{i}(kx_n - \omega t)). \tag{43}$$

Substituting Eq. (43) into the equation of motion of the central particle n, Eq. (37), yields

$$\omega^2 = 4\frac{K}{M}\sin^2\Big(\frac{k\ell}{2}\Big). \tag{44}$$

On the other hand, the dispersion curve of the α-model is obtained by Eq. (8) for $\alpha = \frac{1}{12}$, $\beta = \gamma = 0$, whereas that of the causal model is expressed as [11]

$$\omega^2 = c_e^2 \, \frac{1 + \frac{2}{15}\ell^2 k^2 \pm \sqrt{\left(1 + \frac{2}{15}\ell^2\, k^2\right)^2 - \frac{1}{5}\ell^2\, k^2}}{\frac{1}{10}\ell^2} \tag{45}$$

DOI: 10.1002/nme

that gives rise to two branches in the ω–k plane, a primary (or *acoustical*) branch that passes through the origin (by taking the negative sign of the square root term) and a secondary (or *optical*) branch that starts at a finite cut-off frequency. Only the former branch is considered in the comparison of Fig. 5. The dispersion properties of the three gradient elasticity models are scrutinised in Fig. 5 in terms of dispersion curve $\omega = \omega(\chi)$, where $\chi = k\ell$. As can be seen from this Figure, a significantly better description of the dispersive curve of the discrete medium, Eq. (44), is obtained through the proposed formulation.

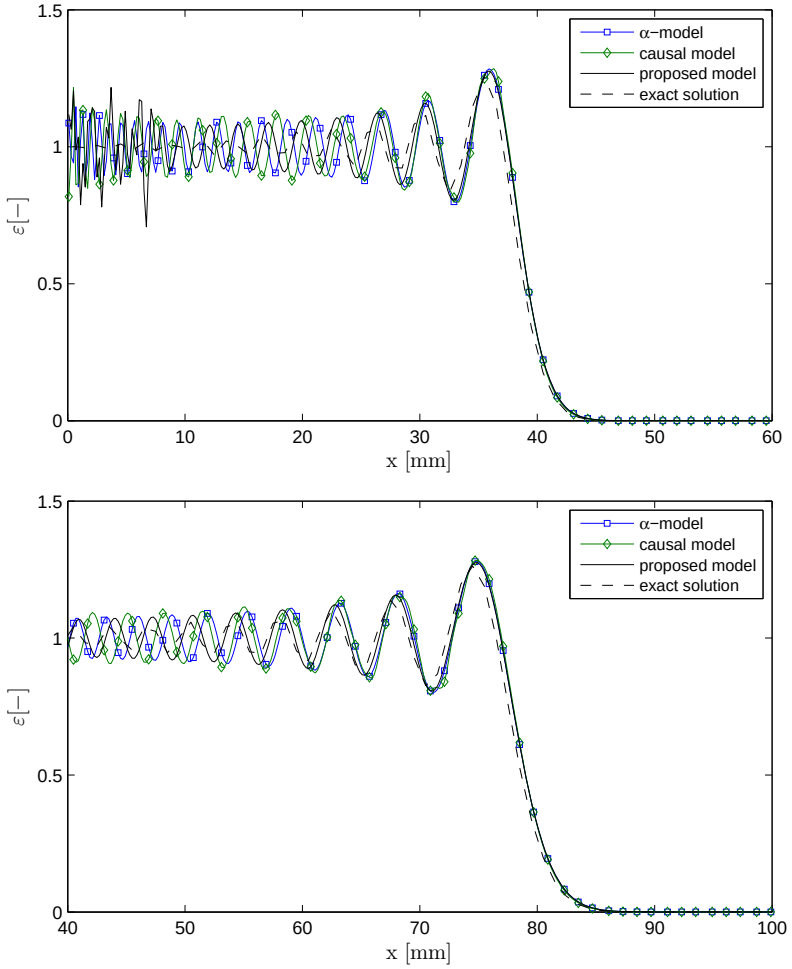

Figure 6. Wave propagation, in terms of ε^M, in a discrete chain of masses and springs simulated with α-model and causal model described in [11] and proposed model compared to the exact solution given in [12] at $t = 40\,\mathrm{s}$ (top) and $t = 80\,\mathrm{s}$ (bottom)

To assess the accuracy of the proposed gradient formulation, we compare the numerical results with a reference solution for this problem. In [12] a semi-infinite cascade of mass-spring systems has been studied that is subjected to a compressive force (that is, directed in the opposite direction as compared to that of Fig. 3) expressed as $F = F_0\,U(t)$, where F_0 is a constant stepforce at time $t = 0$ (we assume $F = 1\,\mathrm{N}$) and the function $U(t)$ represents the Heaviside unit-step function. For the case with a uniform distribution of mass M (we assume $M = 1\,\mathrm{kg}$) and stiffness K (we assume $K = 1\,\mathrm{N/m}$), an exact solution for the acceleration of the n^{th} particle at the time instant t is expressed as [12]

$$\ddot{u}_n(t) = \frac{2n-1}{t} J_{2n-1}(2t) \tag{46}$$

Prepared using nmeauth.cls
DOI: 10.1002/nme

where $J_{2n-1}(2t)$ is the Bessel function of the first kind of order $2n-1$, evaluated at time $2t$. Given the solution in terms of acceleration, a solution in terms of displacements may be found from the equation of motion of the particle n, see Eq. (37). The exact solution obtained via (46) (with a negative sign) has been compared to the solution given by the proposed gradient elasticity model for the problem sketched in Fig. 3. The length of the bar is assumed to be $L = 100\,\mathrm{m}$, the cross-sectional area $A = 1\,\mathrm{m}^2$ and the particle spacing $\ell = 1\mathrm{m}$. By considering the latter parameters and the values of the mass and spring stiffness of the discrete model, $M = 1\,\mathrm{kg}$ and $K = 1\,\mathrm{N/m}$, equivalence of the discrete model (37) and the continuous counterpart (38) implies that $\rho = 1\,\mathrm{kg/m}^3$ and $E = 1\,\mathrm{N/m}^2$. As to the finite element model, the bar is discretised with 500 linear finite elements (element size $h = 0.2\,\mathrm{m}$) and the time step of the Newmark constant average acceleration scheme is taken as $\Delta t = 0.2\,\mathrm{s}$. In Fig. 6 the results obtained by the proposed model are reported in terms of (macroscopic) strain ε^M for two time instants, namely $t = 40\,\mathrm{s}$ and $t = 80\,\mathrm{s}$. In Fig. 6 we have superimposed the numerical results obtained for the same problem by the numerical implementation of the α-model and the causal model discussed above. Note that the discretisation parameters and all the other data of this problem have been chosen so as to allow a consistent comparison with results already published in previous papers, cf. Fig. 5 reported in [11]. By inspection of Fig. 6, we can observe that all the gradient elasticity solutions show a reasonably good agreement with the exact solution of the discrete model. However, especially away from the wave front, the proposed model gives a more accurate prediction of the dispersive wave propagation than the other two gradient elasticity models.

8.2. Periodically heterogeneous composite laminate

Elastic wave propagation through heterogeneous media is generally dispersive due to successive reflection and refraction of the waves between the interfaces of the material (the so-called impedance mismatch zones). In this case attenuation of the wave propagation occurs when the signal travels from one end of the medium to the other, which may be explained by taking into account the interaction between the incident, reflected and transmitted waves at the discontinuity zones. This physical phenomenon is more significant when the wavelength of the travelling signal is comparable to the characteristic length of the microstructure, as noted in Section 1, and cannot be captured by classical elasticity theory that predicts a uniform phase velocity of every individual harmonic component. When impedance mismatch zones (e.g. material discontinuities) are introduced periodically in a medium, interesting wave dynamic characteristics can arise, for instance, one can control the frequency bands over which waves are allowed to pass or stop, the so-called Pass and Stop-bands [34]. In this paper we study the dispersive wave propagation of a composite laminate modelled as a one-dimensional rod of length L (see again Fig. 3), and whose microstructure is depicted in Fig. 7.

The microstructure of the considered composite rod consists of parallel, homogeneous layers alternating periodically along its length. These layers are assumed to be perfectly bonded along plane interfaces across which there is continuity of displacements. Moreover, the composite rod is considered to be very long so that the wave propagation in its periodic layer can be studied by analysing the behaviour of its 'unit cell'. Due to the periodical microstructure of the laminate, piecewise homogeneous material characteristics are assumed: material 1 is defined by mass density ρ_1 and Young's modulus E_1, whereas the analogous quantities for material 2 are denoted as ρ_2 and E_2. The volume fractions of the two materials in each unit cell are governed by the parameter a, with $0 \leq a \leq 1$ (the limits being representative of a homogeneous medium).

Many researchers have made effort to derive effective homogeneous models in which the local fluctuations due to the heterogeneities do not appear explicitly in the equation of motion, see e.g. [3, 4, 17, 21]. Indeed, the study of the original heterogeneous medium can be simulated by a homogeneous one with certain homogenised (so-called *effective*) material properties. Such approximation is more realistic when the microscopic size ℓ of heterogeneities is significantly smaller than the macroscopic length L, at the limit $\epsilon = \ell/L = 0$, where ϵ denotes the rate of heterogeneities of the composite laminate. In reality, $0 < \epsilon \ll 1$ and microstructural scale effects take place that cannot be predicted by simple homogenisation schemes, but higher order asymptotic

DOI: 10.1002/nme

homogenisation approaches are required, i.e. homogenisation with multiple length scales (and/or time scales).

For example, in [3] an effective solution has been obtained by considering the displacements entering the equations of motion as an asymptotic expansion

$$u_i = u_i^{(0)}(x) + \epsilon u_i^{(1)}(x,y) + \epsilon^2 u_i^{(2)}(x,y) + \dots \tag{47}$$

where the first term $u_i^{(0)}(x)$ represents the homogenised part of the solution, and $y = x/\epsilon$ is a microscopic spatial length variable or fast spatial scale, as opposed to the slow coordinate variable x. Therefore, increasingly accurate solutions may be found by considering corrections of $u_i^{(0)}(x)$ of the order ϵ^j by adding next terms $u_i^{(j)}$ (j=1,2,3, ...). These extra terms are necessary to account for local variations of the displacements on the scale of heterogeneities. The macroscopic equation of motion at $\mathcal{O}(1)$, that is, when considering the homogenised part of the solution only, are written as

$$\bar{\rho}\,\ddot{u} = \bar{E}u'' \tag{48}$$

where $\bar{\rho}$ and $\bar{E}$ are the effective mass density and the effective Young's modulus that are related to the component properties through the following relations [3, 17]

$$\bar{\rho} = a\rho_1 + (1-a)\rho_2 \tag{49a}$$

$$\bar{E} = \frac{E_1 E_2}{(1-a)E_1 + aE_2}. \tag{49b}$$

Note that such an effective homogeneous continuum model, up to leading order $\mathcal{O}(1)$, is non-dispersive since the equations of motion (48) are of the same format as in classical elasticity.

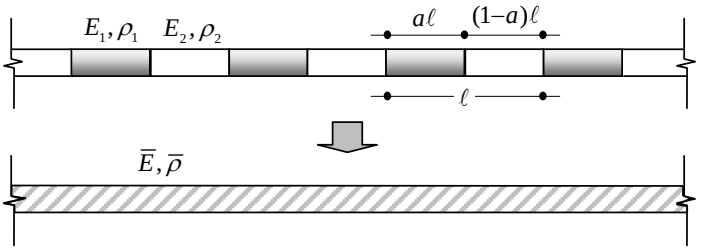

Figure 7. Sketch of a two-component laminate with periodically heterogenous microstructure

By introducing some correction terms in the asymptotic expansion (47), the macroscopic equation of motion at $\mathcal{O}(\epsilon^2)$ reads

$$\bar{\rho}\ddot{u} = \bar{E}\left(u'' + \frac{1}{12}\theta^2\ell^2 u''''\right) + \mathcal{O}(\epsilon^4) \tag{50}$$

where the dimensionless coefficient θ captures the contrast in acoustic impedance of the two materials and is expressed as

$$\theta = \frac{a(1-a)(E_1\rho_1 - E_2\rho_2)}{\bar{\rho}\left((1-a)E_1 + aE_2\right)}. \tag{51}$$

Equation (50) has been derived in [3] and [17,21] by means of different reasonings. The term $\frac{1}{12}\bar{E}\theta^2$ may be considered as the $\mathcal{O}(\epsilon^2)$ effective modulus that characterizes the effect of the microstructure on the macroscopic behaviour. Note that the θ term in the right-hand side of Eq. (50) predicts the effect of wave dispersion caused by the scattering of the global wave at the local heterogeneities of the composite laminate [3]. A non-dispersive medium is obtained when the $\mathcal{O}(\epsilon^2)$ effective modulus vanishes. This occurs either if the material is homogeneous ($a = 0$ or $a = 1$), or if the acoustic impedances of the two components are identical ($E_1\rho_1 = E_2\rho_2$), which means that no wave reflections at the component interfaces take place.

DOI: 10.1002/nme

We are interested in considering a more general formula than Eq. (50) by adding some further contributions in the asymptotic expansions (47). Indeed, to tailor the coefficients of the gradient elasticity model developed in this paper, in particular the β term underlying the additional micro-inertia contribution, we need to take into account higher-order terms up to $\mathcal{O}(\epsilon^4)$. The higher-order homogenisation up to $\mathcal{O}(\epsilon^4)$ has been reported in [20] and reads

$$\bar{\rho}\ddot{u} = \bar{E}\left(u'' + \frac{1}{12}\theta^2\ell^2 u'''' - \frac{1}{360}\theta^2\psi^2\ell^4 u''''''\right) + \mathcal{O}(\epsilon^6) \tag{52}$$

where $\frac{1}{360}\bar{E}\theta^2\psi^2$ may be regarded as the $\mathcal{O}(\epsilon^4)$ effective modulus and the new coefficient ψ is defined as

$$\psi = \frac{\sqrt{c_1}}{\bar{\rho}\left((1-a)E_1 + aE_2\right)} \tag{53a}$$

$$\begin{aligned} c_1 = a^2E_2^2\left[2a^2\rho_1^2 - (1-a)^2\rho_2^2 + 6a(1-a)\rho_1\rho_2\right] + 2a(1-a)E_1E_2\left[3a^2\rho_1^2 + 3(1-a)^2\rho_2^2\right. \\ \left. + 11a(1-a)\rho_1\rho_2\right] - (1-a)^2E_1^2\left[a^2\rho_1^2 - 2(1-a)^2\rho_2^2 - 6a(1-a)\rho_1\rho_2\right]. \end{aligned} \tag{53b}$$

Some mathematical manipulations are required to replace the unstable higher-order stiffness term $\frac{1}{12}\theta^2\ell^2u''''$ with a stable higher-order inertia term and to identify the three coefficients of the developed gradient elasticity model. To this aim, the second space derivative is taken from Eq. (52), the result is multiplied with $\frac{1}{12}(\theta^2+\zeta^2)\ell^2$ (where ζ is a coefficient) and subtracted from Eq. (52). Ignoring terms beyond or including $\mathcal{O}(\epsilon^6)$, the mathematical manipulations described above yield

$$\bar{\rho}\left(\ddot{u} - \frac{1}{12}(\theta^2+\zeta^2)\ell^2\ddot{u}''\right) = \bar{E}\left(u'' - \frac{1}{12}\zeta^2\ell^2u'''' - \frac{1}{720}(2\theta^2\psi^2 + 5\theta^4 + 5\theta^2\zeta^2)\,\ell^4u''''''\right) + \mathcal{O}(\epsilon^6). \tag{54}$$

Since the negative sign of the u'''''' term is destabilising, cf. Eq. (4), we eliminate this term as follows: the fourth space derivative is taken from Eq. (52), the result is multiplied with $\frac{(2\theta^2\psi^2+5\theta^4+5\theta^2\zeta^2)}{720}\,\ell^4$ and added to Eq. (54). Ignoring terms beyond or including $\mathcal{O}(\epsilon^6)$, the mathematical manipulations described above lead to

$$\bar{\rho}\left(\ddot{u} - \frac{1}{12}(\theta^2+\zeta^2)\ell^2\ddot{u}'' + \frac{1}{720}(2\theta^2\psi^2 + 5\theta^4 + 5\theta^2\zeta^2)\,\ell^4\ddot{u}''''\right) = \bar{E}\left(u'' - \frac{1}{12}\zeta^2\ell^2u''''\right) + \mathcal{O}(\epsilon^6). \tag{55}$$

Note that the truncation error of Eqs. (52) and (55) is the same, namely $\mathcal{O}(\epsilon^6)$, but the latter equation contains only stable terms.

The meaning of the ζ coefficient has already been given in other papers, see e.g. [15, 23]. Indeed, if we focus on the term $\frac{1}{12}\zeta^2\ell^2$ on the right-hand side of Eq. (55), this can be assumed as the square of an internal length scale in statics, say ℓ_{stat}^2 (cf. with Eq. (2) of the Aifantis' 1992 strain gradient theory). It has been demonstrated that ℓ_{stat} can be related to the size of the RVE in statics, say L_{RVE}. On the basis of the homogenisation of a RVE of heterogeneous material, it has been found that $\ell_{\text{stat}}^2 \equiv \frac{1}{12}L_{\text{RVE}}^2$ [23] and, thus, one can write

$$\ell_{\text{stat}}^2 = \frac{1}{12}\zeta^2\ell^2 \equiv \frac{1}{12}L_{\text{RVE}}^2. \tag{56}$$

Since the size of the RVE of a strictly periodic laminate is equal to the size of the unit cell, that is, $L_{\text{RVE}} \equiv \ell$, Eq. (56) holds if, and only if, $\zeta = 1$, from which this coefficient is uniquely determined. Substituting the value $\zeta = 1$ into Eq. (55) results in

$$\bar{\rho}\left(\ddot{u} - \frac{1}{12}(\theta^2+1)\ell^2\ddot{u}'' + \frac{1}{720}(2\theta^2\psi^2 + 5\theta^4 + 5\theta^2)\,\ell^4\ddot{u}''''\right) = \bar{E}\left(u'' - \frac{1}{12}\ell^2u''''\right) + \mathcal{O}(\epsilon^6). \tag{57}$$

By comparing Eq. (57) obtained via the higher-order asymptotic expansion of a strictly periodic laminate, and Eq. (5) representing the one-dimensional format of the equation of motion of the proposed enhanced gradient elasticity model, the three model parameters α, β and γ are uniquely

DOI: 10.1002/nme

identified for this problem as

$$\alpha = \frac{1}{12}(\theta^2 + 1), \quad \beta = \frac{1}{720}(2\theta^2\psi^2 + 5\theta^4 + 5\theta^2), \quad \gamma = \frac{1}{12}. \tag{58}$$

Therefore, for the numerical simulation of the dispersive wave propagation occurring in a strictly periodic laminate as depicted in Fig. 7, we assume the effective mass density $\bar{\rho}$ and the effective Young's modulus $\bar{E}$ as given in Eqs. (49), the length scale parameter ℓ is set equal to the size of the unit cell, and the values of α, β and γ are given in (58), where θ is the coefficient given in (51) and ψ is the coefficient given in (53). As a result, all constitutive parameters of the proposed gradient elasticity model are expressed entirely in terms of the properties of the given composite laminate.

The dispersive wave propagation through periodically heterogeneous composite laminates has already been studied in [15] by means of a dynamically consistent gradient elasticity model that is basically the model expressed by Eq. (50) and representing the asymptotic homogenisation up to the $\mathcal{O}(\epsilon^2)$ term. This model contains only the α and γ term of the present formulation and we can retrieve these results by setting $\beta = 0$ in (58). Two periodic laminates with different wave dispersion characteristics were investigated in [15] by varying the material properties of the unit cell. It seems interesting to take into account the material data reported in the mentioned paper so as to make a consistent comparison and to assess the improvements achieved by the proposed formulation.

By assuming a common volume fraction $a = \frac{1}{2}$ for the two laminates, unitary macroscopic (effective) material properties are considered, i.e. $\bar{\rho} = 1\,\mathrm{kg/m^3}$ and $\bar{E} = 1\,\mathrm{N/m^2}$. Therefore, for given properties E_1, ρ_1 of the material 1 the corresponding ones for material 2, namely E_2, ρ_2, are obtained by means of Eqs. (49). The two investigated laminates are characterised by the following properties: (i) the limit case of a laminate with strong contrast between the two materials by considering material 1 as a stiff, dense material, with $E_1 = 10^6\,\mathrm{N/m^2}$ and $\rho_1 = 1.9999\,\mathrm{kg/m^3}$, associated to a contrast of impedance between the two materials $\theta = 0.99995$; (ii) a heterogeneous laminate with weak contrast having $E_1 = 10\,\mathrm{N/m^2}$ and $\rho_1 = 1.2\,\mathrm{kg/m^3}$, associated with $\theta = 0.55$. Note that the stronger the heterogeneities (in terms of impedance mismatch), the more dispersive the wave propagation, therefore we expect a more dispersive behaviour for case (i) than for case (ii).

Before analysing the numerical results obtained for the discretised model, it is interesting to compare the dispersion curve of the proposed model with the exact dispersion curve of the periodically heterogeneous laminate. The latter can be derived by applying the Floquet theorem to the periodic equations of motion (see [14]) and by imposing continuity of displacements and stresses at the interfaces and periodicity of the problem, which results in the following trigonometric dispersion equation [3, 14, 34]

$$\cos(\bar{k}\ell) = \cos(\Omega)\cos(\Omega\tau) - \frac{\xi^2 + 1}{2\xi}\sin(\Omega)\sin(\Omega\tau) \tag{59}$$

where $\bar{k}$ is the effective wave number that quantifies the nature of the wave propagation along the rod. If one introduces the phase velocities in the two materials, c_1 and c_2, and the lengths of the two materials within the unit cell, $L_1 = a\ell$ and $L_2 = (1-a)\ell$, in Eq. (59) $\Omega = \omega L_1/c_1$ is the product of the angular frequency and the time required for the wave to cross one layer of material 1, $\tau = L_2c_1/L_1c_2$ is the ratio of the times taken by a wave to cross the layers of the composite and $\xi = \sqrt{E_1\rho 1}/\sqrt{E_2\rho_2}$ represents the relative impedance of the composite. The exact dispersion curves of the two analysed periodically heterogeneous laminates are reported in Fig. 8 and compared with increasing orders of asymptotic homogenisation of the periodic laminate. More specifically, in Fig. 8 we report the dispersion curves of the non-dispersive $\mathcal{O}(1)$ homogenisation given by Eq. (48), the $\mathcal{O}(\epsilon^2)$ homogenisation given by Eq. (50), which corresponds to the gradient elasticity model discussed in [15], and the proposed model with $\mathcal{O}(\epsilon^4)$ accuracy given by Eq. (52). For the case with strong contrast the proposed model gives a very precise description of the dispersion curve of the heterogeneous medium, and the introduction of the β term leads to significant improvements as compared to the $\mathcal{O}(\epsilon^2)$ gradient model. For the case with weak contrast the accuracy of the proposed model is not as apparent as for the previous laminate, however encouraging improvements are observed when comparing the $\mathcal{O}(\epsilon^4)$ and the $\mathcal{O}(\epsilon^2)$ models.

DOI: 10.1002/nme

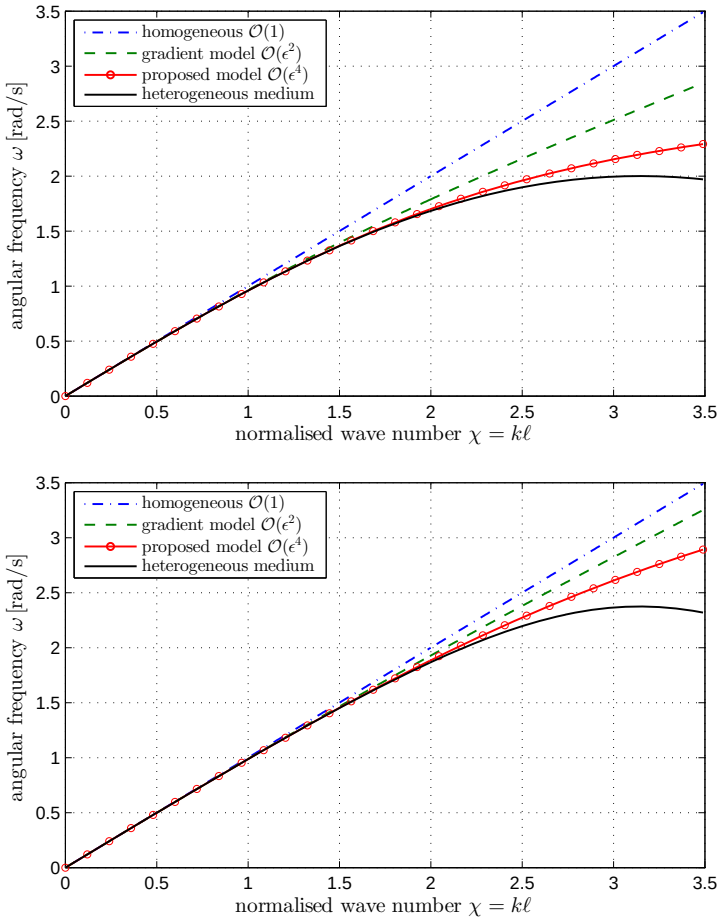

Figure 8. Dispersion curves of periodically heterogeneous laminates with strong contrast (top) and weak contrast (bottom)

To assess the accuracy of the proposed model we compare the numerical results with a reference solution obtained by explicitly modelling the variation of the material properties within the periodically heterogenous laminate. With reference to Fig. 3, we consider a bar having length $L = 300\,\mathrm{m}$ and cross-sectional area $A = 1\,\mathrm{m}^2$. The bar is fixed at the right hand end and subjected to a (compressive) unit-pulse at its left hand end, that is, a force expressed by $F = F_0\,\delta(t)$, with $\delta(t)$ the Dirac's delta and $F_0 = -1\mathrm{N}$ the unit-pulse applied at $t = 0$ (the negative sign is consistent with the direction of the force in the mechanical model sketched in Fig. 3). The bar is discretised with 1500 elements (so assuming a uniform element size $h = 0.2\,\mathrm{m}$ as in the previous example) and the time step of the Newmark constant average acceleration scheme is taken as $\Delta t = 0.2\,\mathrm{s}$. The heterogeneous elastic solution (i.e. the solution in which the microstructure is modelled explicitly) is instead obtained by a more refined finite element model, that is, by using 6000 linear elements of length $0.05\,\mathrm{m}$ with periodically alternating groups of 10 elements having material properties E_1, ρ_1 and E_2, ρ_2. As a result, we assume a unit cell size $\ell = 1\,\mathrm{m}$. The time step for the heterogeneous solution is set equal to $\Delta t = 0.05\,\mathrm{s}$.

In Fig. 9 we can see the profile of the macroscopic displacement $u \equiv u^M$ at $t = 280\,\mathrm{s}$ for the two analysed laminates. As expected, the $\mathcal{O}(1)$ model is non-dispersive, all wave numbers travel with the same phase velocity. The theoretical wave profile in this case should be a Heaviside function, however some numerical dispersion takes place due to the spatial and time discretisation. On the other hand, both the $\mathcal{O}(\epsilon^2)$ and $\mathcal{O}(\epsilon^4)$ predict wave dispersion due to the heterogeneities in the

DOI: 10.1002/nme

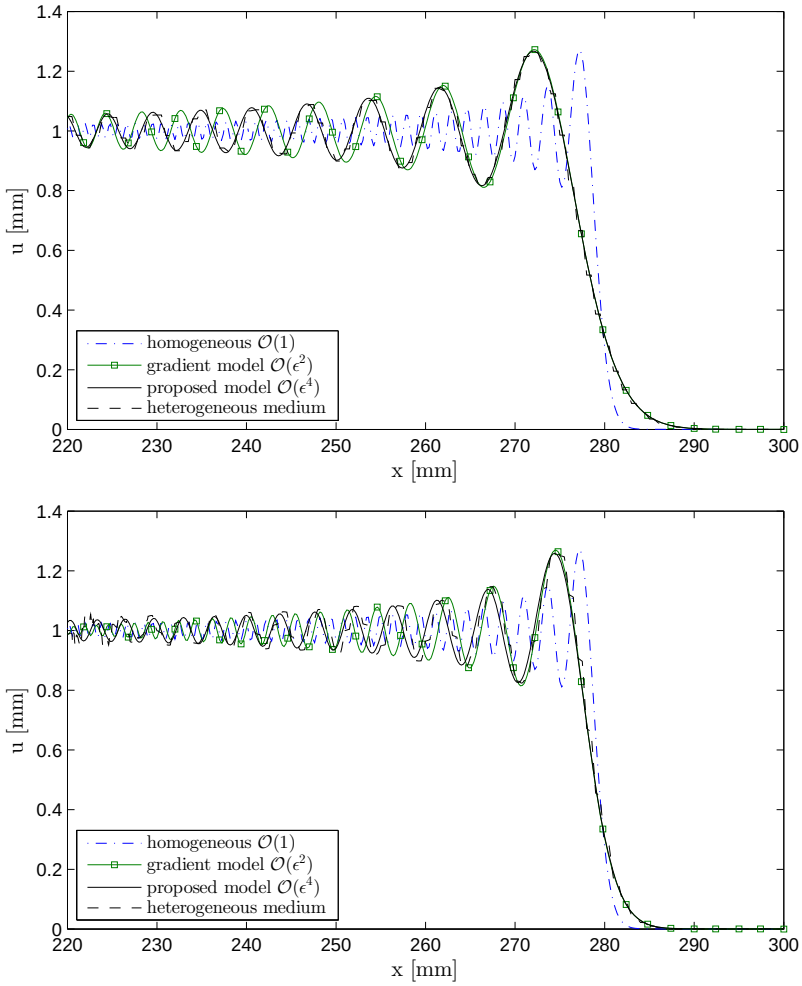

Figure 9. Wave propagation, in terms of u^M, in a periodically heterogeneous laminate with strong (top) and weak contrast (bottom). Simulation with increasing orders of asymptotic homogenisation: homogenous $\mathcal{O}(1)$ as per Eq. (48); gradient model $\mathcal{O}(\epsilon^2)$ given by Eq. (50); proposed model $\mathcal{O}(\epsilon^4)$ given by Eq. (52)

laminate microstructure. Considerable improvements are obtained by the proposed formulation as compared to the $\mathcal{O}(\epsilon^2)$ gradient model discussed in [15] due to the additional micro-inertia contribution. For the case with strong contrast it can be observed that the wave profile of the proposed $\mathcal{O}(\epsilon^4)$ model and that of the heterogeneous model in which the local variations of the material properties are modelled explicitly are basically coincident for a very large range of wave numbers. We emphasize that the former solution is obtained with a significant saving in terms of computational resources and CPU times as compared to the heterogeneous solution owing to the different h and Δt parameters involved in the finite element model. For the case with weak contrast we still obtain some good agreement with the heterogeneous solution, and the improvements of the proposed $\mathcal{O}(\epsilon^4)$ model compared to the $\mathcal{O}(\epsilon^2)$ gradient model are noticeable not only around the wave front but also away from it where the latter model deviates more. However, the accuracy of the gradient solution is less striking than in the previous case, which has already been pointed out when comparing the dispersion curves, cf. Fig. 8. In this regard, it is worth noting that the comparison in terms of dispersion curves serves to assess to what extent the results of the numerical finite element model given in Fig. 9 are reflected and supported in their physical counterpart. These results are definitely consistent with each other.

DOI: 10.1002/nme

9. CONCLUDING REMARKS

In this contribution, a new multi-scale gradient elasticity model has been developed. The proposed model contains *three higher-order terms* (accompanied by three material length scale parameters) that involve both the inertia and the stiffness terms in the equations of motion. As compared to a previous dynamically consistent model containing two gradient terms (a micro-inertia and a strain gradient) [5, 9], the developed model presents *an additional micro-inertia term* that is found to significantly improve the prediction of wave dispersion. The motivations for this model are, in fact, related to experimental observations concerning the dispersion characteristics of materials with a lattice structure. In order to achieve a qualitative match between numerical and experimental dispersion curves, such additional micro-inertia term turn out to be necessary. However, we have proposed a formulation in which this additional term does not imply any extra additional cost from a computational point of view (i.e. with regard to the spatial discretisation and the resulting finite element implementation). Similarly to the earlier dynamically consistent model, the fourth-order equations of motion are split into a set of second-order equations so that the requirement on the interpolation is $\mathscr{C}^0$-continuity rather than $\mathscr{C}^1$-continuity. According to the proposed formulation, the earlier dynamically consistent model with two parameters is retrieved for a zero value of the additional micro-inertia term.

Two sets of unknowns, identified as the displacements at the macroscale and at the microscale, appear simultaneously (i.e. in a coupled fashion) in the resulting split second-order equations, which highlights the multi-scale nature of the proposed formulation. A few mathematical manipulations are introduced to express the coupled equations in a symmetric format. Accordingly, the potential and kinetic energy densities are presented and variationally consistent boundary conditions are derived using the Hamilton-Ostrogradsky principle. The corresponding system matrices in the finite element discretised equations are symmetric and positive-definite provided that certain restrictions on the relative magnitudes between the three material length scale parameters are met. However, we have pointed out that numerical stability of the finite element implementation is guaranteed regardless of these restrictions.

Two simple 1D numerical examples have been analysed to show the effectiveness of the proposed formulation for the prediction of wave dispersion and to highlight the improvements over previous gradient models. A physically meaningful choice of the three material length scales is also discussed so as to link the model coefficients to micro-structural properties. Multi-dimensional examples as well as additional computational aspects of the proposed model will be discussed in a forthcoming study.

APPENDIX A. STABILITY OF THE FINITE ELEMENT IMPLEMENTATION

Even if an unconditionally stable time integration algorithm is adopted to solve the equations of motion of the semi-discretised system, Eqs. (32), numerical instability may arise when the eigenfrequencies of the finite element are not real. It is of interest to check whether such a condition can be obtained when using the proposed finite element implementation and, more importantly, whether some specific conditions are required for this to be avoided, in particular on the three coefficients (α, β, γ) entering the element mass matrix and the element stiffness matrix of the present formulation. In this regard, some conditions have already been derived for guaranteeing positive definitiveness of the kinetic energy, see Section 6.

For the sake of simplicity, we discuss only the one-dimensional case and we assume that the same shape functions for the macroscopic and microscopic displacements are the same, that is, $\mathbf{N}^m \equiv \mathbf{N}^M = \mathbf{N}$. With reference to Eq. (32), the free vibrations of a single finite element are studied through the following linear homogenous equation

$$\mathbf{M}\,\ddot{\mathbf{d}}(t) + \mathbf{K}\,\mathbf{d}(t) = \mathbf{0} \tag{A1}$$

where $\mathbf{d} = [\mathbf{d}^m, \mathbf{d}^M]^T$ is a vector collecting the microscopic and macroscopic displacements representing the degrees of freedom of each finite element and $\mathbf{M}$ and $\mathbf{K}$ are the corresponding

DOI: 10.1002/nme

(element) mass matrix and (element) stiffness matrix whose blocks are reported in (33). Introducing a general harmonic solution $\mathbf{d}(t) = \sum_i \mathbf{v}_i \exp(i\,\omega_i t)$ into Eq. (A1) (where ω_i are the natural vibration frequencies and $\mathbf{v}_i \neq \mathbf{0}$ the corresponding vibration mode shapes) yields the well-known eigenvalue problem in ω_i^2, whose values are determined as the roots of the characteristic polynomial

$$\det[-\omega_i^2\,\mathbf{M} + \mathbf{K}] = 0. \tag{A2}$$

For a two-noded bar element of length h and unitary cross-section, using linear shape functions $\mathbf{N}$, the element (consistent) mass matrix and element stiffness matrix entering the eigenvalue problem (A2) are expressed as (cf. Eqs. (32) and (33))

$$\mathbf{M} = \begin{bmatrix} \left(\frac{\alpha}{\gamma} - \frac{\beta}{\gamma^2}\right)\mathbf{M}_c + \frac{\beta\ell^2}{\gamma}\mathbf{M}_g & -\left(\frac{\alpha}{\gamma} - \frac{\beta}{\gamma^2} - 1\right)\mathbf{M}_c \\ -\left(\frac{\alpha}{\gamma} - \frac{\beta}{\gamma^2} - 1\right)\mathbf{M}_c & \left(\frac{\alpha}{\gamma} - \frac{\beta}{\gamma^2} - 1\right)\left(\mathbf{M}_c + \gamma\ell^2\,\mathbf{M}_g\right) \end{bmatrix}, \quad \mathbf{K} = \begin{bmatrix} \mathbf{K}_c & \mathbf{0} \\ \mathbf{0} & \mathbf{0} \end{bmatrix} \tag{A3}$$

where $\mathbf{0}$ is a 2-by-2 zero matrix, $\mathbf{M}_c$ and $\mathbf{K}_c$ are the classical (consistent) mass matrix and stiffness matrix, respectively, while $\mathbf{M}_g$ is a gradient contribution:

$$\mathbf{M}_c = \frac{\rho h}{6}\begin{bmatrix} 2 & 1 \\ 1 & 2 \end{bmatrix}, \quad \mathbf{K}_c = \frac{E}{h}\begin{bmatrix} 1 & -1 \\ -1 & 1 \end{bmatrix}, \quad \mathbf{M}_g = \frac{\rho}{h}\begin{bmatrix} 1 & -1 \\ -1 & 1 \end{bmatrix}. \tag{A4}$$

One may easily note that using a lumped mass matrix formulation for this format of gradient elasticity would cancel the gradient contribution $\mathbf{M}_g$ and, in turn, would nullify the gradient effects (although some remedies have been proposed to overcome this drawback, e.g. in [26]): indeed, the two displacement fields would be coincident with each other, $\mathbf{d}^m \equiv \mathbf{d}^M$, and would obey the equations of classical elasticity (in other words, the length scale terms would cancel out).

Inserting the expressions of $\mathbf{M}$ and $\mathbf{K}$ given by Eqs. (A3) and (A4) into the eigenvalue problem (A2) leads to the following eigenvalues

$$\begin{aligned} \omega_1^2 = \omega_2^2 = \omega_3^2 = 0 \\ \omega_4^2 = \frac{12c_e^2}{h^2}\left(\frac{1 + 12\,\gamma\left(\frac{\ell}{h}\right)^2}{1 + 12\,\alpha\left(\frac{\ell}{h}\right)^2 + 144\,\beta\left(\frac{\ell}{h}\right)^4}\right) \end{aligned} \tag{A5}$$

where $c_e^2 = E/\rho$ and the zero eigenvalues characterise some rigid body motions (each node being equipped with two degrees of freedom, namely the displacements at the microscale and at the macroscale). It can be observed that the non-zero eigenvalue is always positive, and therefore the corresponding eigenfrequency is always real, for any choice of the model coefficients α, β, γ, provided that these coefficients are positive. It is worth noting that this condition holds true even if the energy functionals are not positive definite. Indeed, if one assumes a set of the three coefficients such that $\alpha \not> \frac{\beta}{\gamma} + \gamma$ (in contrast to the recommendations of Section 6 with regard to the positive-definitiveness of the kinetic energy), the relation $\omega_4 > 0$ still holds true and, thus, numerical stability is not violated.

Finally, since in classical elasticity the non-zero eigenfrequency for a two-noded finite element with linear shape function is $\omega_c^2 = 12c_e^2/h^2$, relation (A5) can be regarded as the eigenfrequency of the classical elasticity multiplied with the bracketed correction factor that is related to the gradient effects.

APPENDIX B. SYMMETRIC FORMULATION OF EQS. (11)

In order to turn Eqs. (11) into a *symmetric* formulation, a few mathematical manipulations are necessary that are listed below:

1) Take the second time derivative of Eq. (11b) and rewrite this equation in terms of accelerations rather than displacements, that is

$$\ddot{u}_i^M - \gamma\ell^2\ddot{u}_{i,nn}^M = \ddot{u}_i^m \tag{B1}$$

DOI: 10.1002/nme

2) Multiply Eq. (B1) with α/γ and use this result to replace the $\alpha\ell^2\ddot{u}^M_{i,nn}$ term in Eq. (11a)

$$\alpha\ell^2\ddot{u}^M_{i,nn} = \frac{\alpha}{\gamma}(\ddot{u}^M_i - \ddot{u}^m_i) \tag{B2}$$

3) Multiply Eq. (B1) with $\beta\ell^2/\gamma$ and derive twice in space so as to obtain a $\beta\ell^4\ddot{u}^M_{i,nnjj}$ term to be used in Eq. (11a)

$$\beta\ell^4\ddot{u}^M_{i,nnjj} = \frac{\beta\ell^2}{\gamma}(\ddot{u}^M_{i,nn} - \ddot{u}^m_{i,nn}) \tag{B3}$$

4) Use Eq. (B1) again to eliminate $\ddot{u}^M_{i,nn}$ from Eq. (B3) as follows

$$\beta\ell^4\ddot{u}^M_{i,nnjj} = \frac{\beta\ell^2}{\gamma}\left[\frac{1}{\gamma\ell^2}(\ddot{u}^M_i - \ddot{u}^m_i) - \ddot{u}^m_{i,nn}\right] = \frac{\beta}{\gamma^2}(\ddot{u}^M_i - \ddot{u}^m_i) - \frac{\beta\ell^2}{\gamma}\ddot{u}^m_{i,nn} \tag{B4}$$

5) Substitute Eq. (B2) and (B4) into Eq. (11a) so as to obtain

$$\rho\left[\ddot{u}^M_i - \frac{\alpha}{\gamma}(\ddot{u}^M_i - \ddot{u}^m_i) + \frac{\beta}{\gamma^2}(\ddot{u}^M_i - \ddot{u}^m_i) - \frac{\beta\ell^2}{\gamma}\ddot{u}^m_{i,nn}\right] = C_{ijkl}\,u^m_{k,jl} \tag{B5}$$

6) Finally, collect terms in the microdisplacements and macrodisplacements in Eq. (B5) and multiply Eq. (B1) with $-\rho\left(\frac{\alpha}{\gamma} - \frac{\beta}{\gamma^2} - 1\right)$ so as to obtain a set of second-order coupled equations that reads

$$\rho\left[\left(\frac{\alpha}{\gamma} - \frac{\beta}{\gamma^2}\right)\ddot{u}^m_i - \frac{\beta\ell^2}{\gamma}\ddot{u}^m_{i,nn} - \left(\frac{\alpha}{\gamma} - \frac{\beta}{\gamma^2} - 1\right)\ddot{u}^M_i\right] = C_{ijkl}\,u^m_{k,jl} \tag{B6a}$$

$$\rho\left[-\left(\frac{\alpha}{\gamma} - \frac{\beta}{\gamma^2} - 1\right)\ddot{u}^m_i + \left(\frac{\alpha}{\gamma} - \frac{\beta}{\gamma^2} - 1\right)\ddot{u}^M_i - \left(\alpha - \frac{\beta}{\gamma} - \gamma\right)\ell^2\ddot{u}^M_{i,nn}\right] = 0 \tag{B6b}$$

which is the sought symmetric formulation of Eqs. (11).

REFERENCES

1. Aifantis EC. On the role of gradients in localization of deformation and fracture. *International Journal of Engineering Science* 1992; **30**:1279–1299.
2. Altan B, Aifantis EC. On some aspects in the special theory of gradient elasticity. *Journal of the Mechanical Behavior of Materials* 1997; **8**: 231-282.
3. Andrianov I, Bolshakov V, Danishevskyy V, Weichert D. Higher order asymptotic homogenization and wave propagation in periodic composite materials. *Proceeding of the Royal Society A* 2008; **464**:1181-1201.
4. Andrianov I, Awrejcewicz J, Danishevskyy V, Weichert D. Wave propagation in periodic composites: Higher-order asymptotic analysis versus plane-wave expansions method. *Journal of Computational and Nonlinear Dynamics* 2011; **6**:011015.
5. Askes H, Aifantis EC. Gradient elasticity theories in statics and dynamics - a unification of approaches. *International Journal of Fracture* 2006; **139**:297-304.
6. Askes H, Gutiérrez MA. Implicit gradient elasticity. *International Journal for Numerical Methods in Engineering* 2006; **67**:400–416.
7. Askes H, Morata I, Aifantis EC. Finite element analysis with staggered gradient elasticity. *Computers and Structures* 2008; **86**:1266-1279.
8. Askes H, Aifantis EC. Gradient elasticity in statics and dynamics: an overview of formulations, length scale identification procedures, finite element implementations and new results. *International Journal of Solids and Structures* 2011; **48**:1962-1990.
9. Askes H, Bennett T, Aifantis EC. A new formulation and $\mathscr{C}^0$-implementation of dynamically consistent gradient elasticity. *International Journal for Numerical Methods in Engineering* 2007; **72**:111-126.
10. Askes H, Metrikine AV. One-dimensional dynamically consistent gradient elasticity models derived from a discrete microstructure. Part 2: Static and dynamic response. *European Journal of Mechanics – A/Solids* 2002; **21**:573–588.
11. Askes H, Metrikine AV, Pichugin A, Bennett T. Four simplified gradient elasticity models for the simulationof dispersive wave propagation. *Philosophical Magazine* 2008; **88**:3415–3443.
12. Bavinck H, Dieterman HA. Closed-form dynamic response of damped mass–spring cascades *Journal of Computational and Applied Mathematics* 2000; **114**:291–303.

13. Bažant ZP, Jirásek M. Nonlocal integral formulations of plasticity and damage: survey of progress. *Journal of Engineering Mechanics* 2002; **11**:1119–1149.
14. Bedford A, Drumheller DS. *Introduction to Elastic Wave Propagation*. Wiley, New York 1994.
15. Bennett T, Gitman IM, Askes H. Elasticity theories with higher-order gradients of inertia and stiffness for the modelling of wave dispersion in laminates. *International Journal of Fracture* 2007; **148**:185–193.
16. Chang CS, Gao J. Second-gradient constitutive theory for granular material with random packaging structure. *International Journal of Solids and Structures* 1995; **32**:2279-2293.
17. Chen W, Fish J. A dispersive model for wave propagation in periodic heterogeneous media based on homogenization with multiple spatial and temporal scales. *Journal of Applied Mechanics* 2001; **68**:153-161.
18. Engel G, Garikipati K, Hughes TJR, Larson MG, Mazzei L, Taylor RL. Continuous/discontinuous finite element approximations of fourth-order elliptic problems in structural and continuum mechanics with applications to thin beams and plates, and strain gradient elasticity. *Computer Methods in Applied Mechanics and Engineering* 2002; **191**:3669–3750.
19. Eringen AC. On differential equations of nonlocal elasticity and solutions of screw dislocation and surface waves. *Journal of Applied Physics* 1983; **54**:4703–4710.
20. Fish J, Chen W. Higher-order homogenization of initial/boundary-value problem. *Journal of Engineering Mechanics* 2001; **127**:1223–1230.
21. Fish J, Chen W, Nagai G. Non-local dispersive model for wave propagation in heterogeneous media: one-dimensional case. *International Journal for Numerical Methods in Engineering* 2002; **54**:331–346.
22. Fuschi P, Pisano AA, De Domenico D. Plane stress problems in nonlocal elasticity: finite element solutions with a strain-difference-based formulation. *Journal of Mathematical Analysis and Applications* 2015; **431**:714–736.
23. Gitman IM, Askes H, Aifantis EC. The representative volume size in static and dynamic micro-macro transitions. *International Journal of Fracture* 2005; **135**:L3–L9.
24. Gutkin MY, Aifantis EC. Screw dislocation in gradient elasticity. *Scripta Materialia* 1996: **35**:1353–1358.
25. Gutkin MY, Aifantis EC. Edge dislocation in gradient elasticity. *Scripta Materialia* 1997: **36**:129–135.
26. Lombardo M, Askes H. Lumped mass finite element implementation of continuum theories with micro-inertia. *International Journal for Numerical Methods in Engineering* 2013; **96**:448–466.
27. Maugin GA, Metrikine AV. (Eds.). *Mechanics of Generalized Continua One Hundred Years After the Cosserats*. Springer, New York. 2010.
28. Metrikine AV, Askes H. One-dimensional dynamically consistent gradient elasticity models derived from a discrete microstructure. Part 1: Generic formulation. *European Journal of Mechanics – A/Solids* 2002; **21**:555–572.
29. Metrikine AV, Askes H. An isotropic dynamically consistent gradient elasticity model derived from a 2D lattice. *Philosophical Magazine* 2006; **86**:3259–3286.
30. Mindlin R. Micro-structure in linear elasticity. *Archive for Rational Mechanics and Analysis* 1964; textbf16:51–78.
31. Peerlings RHJ, de Borst R, Brekelmans WAM, de Vree JHV, Spee I. Some observations on localisation in non-local and gradient damage models. *European Journal of Mechanics A/Solids* 1996; **15**:937–953.
32. Polizzotto C, Fuschi P, Pisano AA. A nonhomogeneous nonlocal elasticity model. *European Journal of Mechanics A/Solids* 2006; **25**: 308–333.
33. Ru CQ, Aifantis EC. A simple approach to solve boundary-value problems in gradient elasticity. *Acta Mechanica* 1993; **101**:59–68.
34. Ruzzene M, Baz A. Control of wave propagation in periodic composite rods using shape memory inserts. *Journal of Vibration and Acoustics* 2000; **122**:151–159.
35. Silling SA. Reformulation of elasticity theory for discontinuities and long-range forces. *Journal of the Mechanics and Physics of Solids* 2000; **48**:175-209.
36. Triantafyllidis N, Aifantis EC. A gradient approach to localization of deformation. I. Hyperelastic materials. *Journal of Elasticity* 1986; **16**:225-237.
37. Warren J, Yarnell J, Dolling G, Cowley R. Lattice dynamics of diamond. *Physical Review* 1967; **158**:805–808.
38. Washizu K. *Variational Methods in Elasticity and Plasticity* Pergamon, Oxford. 1975.
39. Yarnell J, Warren J, Wenzel R. Lattice vibrations in diamond. *Physical Review Letters* 1964; **13**:13–15.
40. Yarnell J, Warren J, Wenzel R, Koenig S. Phonon dispersion curves in bismuth. *IBM Journal of Research and Development* 1964; **8**:234–240.
41. Yarnell J, Warren J, Koenig S. Experimental dispersion curves for phonons in aluminium. In: *Lattice Dynamics - Proceedings of an International Conference*, Wallis RF (Eds.), Pergamon Press 1965; 57–61.
42. Zervos A. Finite elements for elasticity with microstructure and gradient elasticity. *International Journal for Numerical Methods in Engineering* 2008; **73**:564–595.
43. Zervos A, Papanicolopulos SA, Vardoulakis I. Two finite element discretizations for gradient elasticity. *Journal of Engineering Mechanics* 2009; **135**:203–213.

DOI: 10.1002/nme